

Published in final edited form as:

Nature. 2020 May 01; 581(7808): 316–322. doi:10.1038/s41586-020-2282-0.

## TASL is the SLC15A4-associated adaptor for IRF5 activation by TLR7-9

Leonhard X. Heinz<sup>1</sup>, JangEun Lee<sup>2</sup>, Utkarsh Kapoor<sup>1</sup>, Felix Kartnig<sup>1</sup>, Vitaly Sedlyarov<sup>1</sup>, Konstantinos Papakostas<sup>1</sup>, Adrian César-Razquin<sup>1</sup>, Patrick Essletzbichler<sup>1</sup>, Ulrich Goldmann<sup>1</sup>, Adrijana Stefanovic<sup>1</sup>, Johannes W. Bigenzahn<sup>1</sup>, Stefania Scorzoni<sup>1</sup>, Mattia D. Pizzagalli<sup>1</sup>, Ariel Bensimon<sup>1</sup>, André C. Müller<sup>1</sup>, F. James King<sup>2</sup>, Jun Li<sup>2</sup>, Enrico Girardi<sup>1</sup>, M. Lamine Mbow<sup>2</sup>, Charles E. Whitehurst<sup>2</sup>, Manuele Rebsamen<sup>1,\*</sup>, Giulio Superti-Furga<sup>1,3,\*</sup>

<sup>1</sup>CeMM Research Center for Molecular Medicine of the Austrian Academy of Sciences, 1090 Vienna, Austria

<sup>2</sup>Boehringer Ingelheim Pharmaceuticals, Ridgefield, 06877 Connecticut, USA

<sup>3</sup>Center for Physiology and Pharmacology, Medical University of Vienna, 1090 Vienna, Austria

### Abstract

Toll-like receptors (TLRs) have a crucial role in the recognition of pathogens and initiation of immune responses<sup>1–3</sup>. Here we show that a previously uncharacterized protein encoded by *CXorf21*—a gene that is associated with systemic lupus erythematosus<sup>4,5</sup>—interacts with the endolysosomal transporter SLC15A4, an essential but poorly understood component of the endolysosomal TLR machinery also linked to autoimmune disease<sup>4,6–9</sup>. Loss of this type-I-interferon-inducible protein, which we refer to as ‘TLR adaptor interacting with SLC15A4 on the lysosome’ (TASL), abrogated responses to endolysosomal TLR agonists in both primary and transformed human immune cells. Deletion of SLC15A4 or TASL specifically impaired the activation of the IRF pathway without affecting NF- $\kappa$ B and MAPK signalling, which indicates that ligand recognition and TLR engagement in the endolysosome occurred normally. Extensive mutagenesis of TASL demonstrated that its localization and function relies on the interaction with SLC15A4. TASL contains a conserved pLxIS motif (in which p denotes a hydrophilic residue and x denotes any residue) that mediates the recruitment and activation of IRF5. This finding shows that TASL is an innate immune adaptor for TLR7, TLR8 and TLR9 signalling, revealing a clear

Users may view, print, copy, and download text and data-mine the content in such documents, for the purposes of academic research, subject always to the full Conditions of use: [http://www.nature.com/authors/editorial\\_policies/license.html#terms](http://www.nature.com/authors/editorial_policies/license.html#terms)

\***Corresponding Authors:** Lead contact: Giulio Superti-Furga, CeMM Research Center for Molecular Medicine of the Austrian Academy of Sciences, Lazarettgasse 14, AKH BT25.3, 1090 Vienna, Austria, [gsuperti@cemm.oeaw.ac.at](mailto:gsuperti@cemm.oeaw.ac.at), Telephone: +43 1 40160 70 001. Manuele Rebsamen, CeMM Research Center for Molecular Medicine of the Austrian Academy of Sciences, Lazarettgasse 14, AKH BT25.3, 1090 Vienna, Austria, [mrebsamen@cemm.oeaw.ac.at](mailto:mrebsamen@cemm.oeaw.ac.at), Telephone: +43 1 40160 70 050.

#### Author contributions

L.X.H., J.E.L., E.G., M.L.M., C.W., M.R., and G.S-F. designed research; L.X.H., J.E.L., U.K., K.P., F.K., P.E., A.S., S.S., A.C.M., F.J.K., M.D.P., E.G. and M.R. performed research; V.S., A.C-R. and U.G. performed bioinformatic analysis; J.W.B., A.B. and J.L. generated reagents and provided scientific insight; L.X.H., M.R. and G.S-F. analyzed and interpreted the data; L.X.H., M.R. and G.S-F. wrote the paper.

#### Competing interests

J.E.L., J.L. J.K., M.L.M. and C.W. are employed in the Immunology & Respiratory department, Drug Concept Discovery group of Boehringer-Ingelheim. The work in the Superti-Furga laboratory is supported by Boehringer-Ingelheim (Grant Agreement 238114).

mechanistic analogy with the IRF3 adaptors STING, MAVS and TRIF<sup>10,11</sup>. The identification of TASL as the component that links endolysosomal TLRs to the IRF5 transcription factor via SLC15A4 provides a mechanistic explanation for the involvement of these proteins in systemic lupus erythematosus<sup>12–14</sup>.

## Keywords

TASL; CXorf21; Toll-like receptors; Solute carriers; IRF5; SLC15A4; autoimmunity

Eukaryotic cells recognize a large variety of pathogens with a limited set of receptors, adaptors and signaling molecules employed in modular and combinatorial fashion, integrating information on subcellular localization and metabolism, to trigger appropriate responses<sup>15–17</sup>. While endolysosomal TLRs have evolved to respond to microbial nucleic acids of various origin, aberrant activation can contribute to development of autoimmunity<sup>2</sup>. Indeed, many pathway components are genetically linked to disease predisposition, such as in the case of SLE<sup>12–14</sup>. We studied the member of the solute carrier family SLC15A4, which has been implicated in endolysosomal TLR activation and autoimmune diseases by mouse models and human genetics, but whose mechanistic role and hierarchical position in the pathway was not yet fully elucidated<sup>4,6–9,18–23</sup>. The human THP1 monocytic cell line expresses both lysosomal SLC15 family members, SLC15A3 and SLC15A4 (Extended Data Fig. 1a). CRISPR/*Cas9*-mediated inactivation of SLC15A4 abrogated TNF production upon stimulation with the TLR7/8-specific agonist R848, demonstrating a non-redundant role for SLC15A4 in human monocytic cells (Fig. 1a). To gain a mechanistic understanding of how SLC15A4 affects this process, we set out to identify its binding partners by interaction proteomics using tandem-affinity purification (TAP) coupled to gel-free liquid chromatography tandem mass spectrometry (LC–MS/MS)<sup>24,25</sup>. We generated THP1 cells stably expressing tagged lysosomal SLC15A4 wild type glycoprotein, a construct lacking a large cytosolic loop ( 253-303) or deleted for the cytosolic N-terminus (aa 1-28, N), which harbors a previously described di-leucine-containing lysosomal sorting signal (LL14-15AA) and therefore mis-localized to the plasma membrane (Extended Data Fig. 1b-e)<sup>7,26</sup>. TAP-MS/MS analysis of these variants provided a global view of the SLC15A4 interaction landscape, and revealed CXorf21, an uncharacterized 301 amino acid protein conserved in vertebrates, as a prominent and specific binder (Fig. 1b, Extended Data Fig. 2a, Supplementary Table 1). *CXorf21* is an X chromosome-encoded gene, which has also been genetically linked to SLE and hypothesized to contribute to the sexual dimorphism of the disease<sup>4,5,27,28</sup>. Based on the evidence presented here, we refer to the protein encoded by the *CXorf21* gene as TASL, TLR Aaptor interacting with SLC15A4 on the Lysosome. While SLC15A4 shows a wider tissue distribution, TASL appears to be restricted to the hematopoietic compartment, in particular to myeloid cells, B lymphocytes and plasmacytoid dendritic cells (DCs) (Extended Data Fig. 2b,c, Supplementary Table 2)<sup>29–31</sup>. Furthermore, TASL and, to a lesser extent, SLC15A4 expression was induced by interferon  $\beta$  treatment (Fig. 1c, Extended Data Fig. 3a,b). Considering the relevance of type I interferons in SLE<sup>12,14,32</sup>, we further confirmed interferon-inducibility in primary human monocyte-derived macrophages and DCs (Fig. 1d). Together, these data suggested that TASL could be exquisitely involved in immune-specific SLC15A4 function.

Next we characterized the SLC15A4-TASL protein complex. TAP-MS/MS analysis using TASL as bait identified endogenous SLC15A4 (Fig. 1e). Conversely, tagged SLC15A4 immunoprecipitated endogenous TASL in different cellular systems (Fig. 1f, Extended Data Fig. 3c). SLC15A4-binding required the N-terminal region of TASL (Fig. 1g, Extended Data Fig. 3d). Demonstrating endogenous complex formation and specificity, TASL was detected in SLC15A4 immunoprecipitates from wild type but not SLC15A4-deficient cells, nor upon immunoprecipitation of lysosomal SLC38A9, which recovered its binding partner RAGA (Fig. 1h, Extended Data Fig. 1d)<sup>24</sup>. SLC15A4, but not the closely related SLC15A3, interacted with TASL (Fig. 1f, Extended Data Fig. 1d, 3e,h). Mutant forms of SLC15A4 ( N and LL14-15AA) that mislocalize to the plasma membrane retained binding and led to the accumulation of a phosphatase-sensitive, slower migrating form of TASL, indicating that the interaction was independent of the subcellular context (Fig. 1f, Extended Data Fig. 1d, 3f). In contrast, a point mutation affecting a conserved glutamate residue previously shown to be required for substrate binding/transport (E465K)<sup>9</sup> resulted in complete loss of TASL binding, raising the possibility that the interaction is conformation-dependent (Fig. 1f, Extended Data Fig. 1b,d,e). Expression of SLC15A4 constructs able to bind TASL resulted in an increase in its abundance, while SLC15A4 knockout cells showed reduced endogenous TASL protein levels (Fig. 1f,2a, Extended Data Fig. 3c,5e). Furthermore, co-expression of wild type SLC15A4 or SLC15A4 N in THP1 cells stably expressing TASL-GFP led to a strong increase in GFP signal and to its recruitment to endolysosomal structures or the plasma membrane, respectively (Extended Data Fig. 4a-d). In contrast, co-expression of SLC15A4 E465K only marginally affected TASL-GFP levels or localization. Together, these experiments revealed a proteostatic relationship regulating TASL abundance depending on SLC15A4 expression levels and binding.

Next, we assessed the relevance of the SLC15A4-TASL module for TLR-induced inflammatory responses. While no major effects were observed on steady-state gene expression, SLC15A4 and TASL deficiency blunted transcriptional responses to R848 stimulation (Fig. 2a-d, Extended Data Fig. 5a-c, Supplemental Table 3). Mirroring SLC15A4 knockouts, TASL-deleted cells showed a strong impairment in R848-induced production of cytokines/chemokines, PD-L1 (CD274) upregulation as well as activation of pathway-specific reporters (Fig. 2e,f, Extended Data Fig. 5d-f). Similar defects were observed using other TLR8 ligands, while knockout cells responded normally to agonists of plasma membrane-localized TLR2 and TLR5, as well as of the STING-dependent cytoplasmic DNA-sensing pathway, demonstrating the specificity of TASL-SLC15A4 for endolysosomal TLRs (Fig. 2e, Extended Data Fig. 5f,g). In contrast to SLC15A4, knockout of the related SLC15A2 and SLC15A3 did not impair R848-induced responses (Extended Data Fig. 5h). The response to type I interferon was intact in TASL/SLC15A4-deficient cells, indicating that impaired interferon signaling is not the underlying cause of the observed phenotypes (Extended Data Fig. 5i). Additionally, no defects in NOD1/2 responses were detected in the absence of TASL or SLC15A4, possibly because of other transporters acting redundantly to mediate ligand uptake (Extended Data Fig. 5f,j,k)<sup>8,26,33,34</sup>. In order to further define the relevance of the TASL-SLC15A4 module, we investigated primary human cells. Knockdown of SLC15A4 and, even more prominently, TASL resulted in reduction of TNF production

upon R848 stimulation of primary CD14<sup>+</sup> monocytes, highlighting the role of the complex for endolysosomal TLR responses (Fig. 2g,h, Extended Data Fig. 5l).

Similarly to TLR7/8, TLR9, the other endolysosomal TLR linked to SLC15A4<sup>7</sup>, plays a central role in physiological and pathological immune responses<sup>2</sup>. While THP1 cells respond poorly to TLR9 agonists, stable expression of the receptor resulted in secretion of pro-inflammatory mediators and interferon  $\beta$  upon CpG-A/B stimulation (Extended Data Fig. 6a,b). Deletion of SLC15A4 or TASL profoundly impaired all these responses (Fig. 3a, Extended Data Fig. 6a,c). SLC15A4/TASL-deficient cells did not display overt defects in TLR protein levels, processing or lysosomal protein abundance nor any detectable alterations in ligand uptake or lysosomal acidification (Extended Data Fig. 6a,d-k). Monitoring endolysosomal TLR-induced signaling, STAT1 activation, likely induced by paracrine interferon, was strongly diminished in SLC15A4 and TASL knockout cells upon both CpG or R848 treatment (Fig. 3b, Extended Data Fig. 6l). Interestingly, no major defect in NF- $\kappa$ B and MAPK pathway activation was detected, indicating that TLR engagement occurred normally in TASL-/SLC15A4-deficient cells, placing the complex downstream of early ligand-receptor activation events (Fig. 3b, Extended Data Fig. 6l). Altogether these data suggested a defect in IRF pathway activation and pointed to a possible involvement of IRF5 given both its role in TLR7-9-mediated induction of proinflammatory mediators and type I interferons as well as its clear association with SLE<sup>35-39</sup>. Indeed, knockout of IRF5, but not of IRF3 or IRF7, specifically compromised responses to endolysosomal TLR agonists in THP1 cells (Extended Data Fig. 7a-g). Accordingly, IRF5 deficiency had the strongest impact on CpG-induced gene expression (Fig. 3c, Extended Data Fig. 7h, Supplementary Table 4). Assessing IRF5 activation upon CpG stimulation, we observed that loss of SLC15A4 or TASL impaired IRF5 phosphorylation (Fig. 3b). Importantly, defects in CpG-induced transcriptional responses observed in TASL/SLC15A4 knockouts mirrored the ones of IRF5-deficient cells, strongly supporting an epistatic relationship between the function of the SLC15A4-TASL complex and IRF5 (Fig 3d-f, Extended Data Fig. 7h-j). Indeed, genes affected by TASL/SLC15A4-deficiency were enriched in IRF targets, while this was not the case in the subset of unaffected transcripts, which displayed an NF- $\kappa$ B-related signature (Fig. 3f, Extended Data Fig. 7j,k).

Plasmacytoid DCs are major producers of type I interferons, respond efficiently to endosomal TLR activation and contribute to SLE pathogenesis<sup>13,32</sup>. In light of this and the described role of SLC15A4 in these cells<sup>7,18,19</sup>, we investigated the function of the SLC15A4/TASL complex in the human pDC cell line CAL-1<sup>35,40,41</sup>. Knockout cells displayed impaired cytokine production upon activation of endogenous TLR7-9, which was associated with a specific defect in IRF5 but not NF- $\kappa$ B/MAPK activation, perfectly in line with phenotypes observed in THP1 monocytes (Fig. 3g-i; Extended Data Fig. 8a-g). To define the molecular mechanism by which the TASL-SLC15A4 complex controls IRF5-dependent endolysosomal TLR signaling, we reconstituted knockout cells. Expression of wild type SLC15A4, but not SLC15A3, rescued the impaired R848 responses as well as the diminished TASL levels (Fig. 4a, Extended Data Fig. 8h,i). This required the SLC15A4 transmembrane core (Extended Data Fig. 8h,i). SLC15A4 variants that localize to the plasma membrane rescued TASL protein abundance, but not signaling (Fig. 4a). Both TASL binding and proper localization were required to restore endolysosomal TLR responses, as

the SLC15A4 E465K mutant failed to rescue knockout cells (Fig. 3i, 4a). Furthermore, substitution of E465 to alanine confirmed the critical involvement for this residue in both TASL-binding and function (Extended Data Fig. 8j). In contrast, mutation of glutamate residues (E44 or E47) in the conserved EXXER motif, previously shown to be required for proton-coupled transport in multiple related transporters<sup>42</sup>, retained TASL-binding and functional rescuing capabilities. These data suggest the requirement for TASL-binding, but not necessarily transport activity of SLC15A4 for endosomal TLR function (Extended Data Fig. 8j). We next profiled the entire TASL protein sequence using a series of 50 sequential mutants in which polar residues were exchanged to alanine and stably expressed in knockout cells (Extended Data Fig. 9a-d). This identified several evolutionary conserved elements that were functionally required (Fig. 4b). While the N-terminal mutant (#1, aa 1-8) failed to bind to endogenous SLC15A4, the interaction was retained by defective mutants affecting the central (#18-21, aa 106-128) and the C-terminal (#34-49, aa 204-296) region, suggesting a role for these elements in mediating TASL effector function (Fig. 4b, Extended Data Fig. 9e). Accordingly, TASL functionality was compromised by either N- or C-terminal tagging (Extended Data Fig. 9f). Sequence analysis of the C-terminal region of TASL revealed homology with the IRF5 C-terminal domain, which is required for phosphorylation-induced activation/dimerization (Fig. 4c,d)<sup>43,44</sup>. Upon inspection of the homologous region of TASL we identified a highly conserved *p*LXIS motif, which in the canonical innate adaptors STING, MAVS and TRIF mediates the phosphorylation-dependent homotypic recruitment and activation of IRF3 downstream of their respective pattern recognition receptors (Fig. 4e)<sup>10,11</sup>. Together with the defects we observed in IRF5 activation, this strongly suggested an analogous role for TASL as innate immune adaptor for IRF5 downstream of endolysosomal TLRs. Indeed, immunoprecipitation of the SLC15A4/TASL complex revealed CpG-induced recruitment of IRF5 (Fig. 4f-h, Extended Data Fig. 9g). Binding was lost both upon TASL knockout or use of the TASL binding-deficient SLC15A4 E465K mutant (Fig. 4f-h). Detailed mutagenesis of the TASL *p*LxIS motif demonstrated strong functional analogy to IRF3 adaptors STING, MAVS and TRIF. Indeed, mutation of the *p*LxIS motif or the core serine S294 abrogated TASL function, with a phosphomimetic S294D substitution retaining detectable activity (Fig. 4i,j). As in STING and MAVS, mutation of serine/threonine clusters preceding the *p*LxIS motif also abrogated its function, while targeting of succeeding residues had no impact (Fig. 4i)<sup>10</sup>. In line with this data, docking of the TASL LxIS-containing peptide onto the IRF5 structure suggested that this peptide would bind to IRF5 through extensive interactions mediated by the motif residues, adopting a similar binding mode as observed in complexes of IRF3 with *p*LxIS-containing peptides of STING, MAVS and TRIF (Extended Data Fig. 9h-k)<sup>11</sup>. TASL functionality was retained when its *p*LXIS motif (SLHIS) was substituted with the corresponding sequences of IRF3 adaptors as well as IRF3 itself, while the IRF5 motif swap mutant was less active (Extended Data Fig. 9l,m). The functional mutants activated IRF5 and not IRF3, indicating that other structural determinants confer IRF specificity.

To understand how TLR engagement signals to the SLC15A4/TASL complex and TASL *p*LXIS-dependent IRF5 activation, we investigated kinases associated with this pathway. Both TBK1/IKK $\epsilon$  and IKK $\beta$  kinases were shown to be involved in IRF3 adaptor phosphorylation and IRF3/5 activation<sup>10,35,45,46</sup>. Similar as shown for IRF5<sup>35</sup>, co-expression

of TASL with these kinases, but not kinase dead mutants, resulted in a migratory shift indicative of hyperphosphorylation (Extended Data Fig. 10a). Treatment with IKK $\beta$  inhibitor TPCA-1 blocked R848-induced responses, IRF5 recruitment and activation, while TBK1/IKK $\epsilon$  inhibitor BX795 was less effective (Extended Data Fig. 10b-d). Furthermore, genetic ablation of IKK $\beta$  as well as upstream kinases IRAK4 and TAK1 abrogated these responses, while TBK1, IKK $\epsilon$  or IKK $\alpha$  inactivation had no or only partial effects (Extended Data Fig. 10e-g). These data support a central role for IKK $\beta$  in TASL-dependent IRF5 activation.

Altogether, the work presented here identifies the complex between the previously uncharacterized protein TASL and SLC15A4, both genetically associated with SLE, as a functional module required for endolysosomal TLR signaling (Fig. 4k). In contrast to what could have been anticipated for an endolysosomally-localized member of a transporter family, deficiency of neither SLC15A4 nor its partner TASL affected ligand-receptor engagement. Rather, loss of their function selectively impaired IRF5 signaling, leaving NF- $\kappa$ B or MAPK induction unaltered. The identification of a functional *pLxIS* motif in TASL unmasked its role as innate immune adaptor required for recruitment and activation of IRF5 by TLR7-9, displaying a remarkable mechanistic analogy with IRF3 and its three adaptors STING, MAVS and TRIF (Fig. 4k, Extended Data Fig. 10h)<sup>10</sup>. In light of these findings, our study provides a molecular explanation for the involvement of TASL and SLC15A4 in SLE, defining the role of the complex in connecting endosomal TLRs to IRF5, both established factors in autoimmune disease, and highlighting its potential as target for pharmaceutical intervention.

## Methods

### Antibodies and reagents

HA (#3724), V5 (#13202), GFP (#2956), RAGA (#4357), TLR9 (#5845), TAK1 (#4505), IRAK4 (#4363), IKK $\alpha$  (#2682), IKK $\beta$  (#8943), TBK1 (#51872), IKK $\epsilon$  (#2905), IRF3 (#11904), IRF7 (#4920), phospho-IKK $\alpha$ / $\beta$  Ser176/180 (#2697), phospho-I $\kappa$ B $\alpha$  Ser32/36 (#9246), phospho-NF- $\kappa$ B p65 Ser536 (#3033), phospho-p38 MAPK Thr180/Tyr182 (#9211), phospho-SAPK/JNK Thr183/Tyr185 (#4668) and phospho-STAT1 Y701 (#7649) antibodies were from Cell Signaling; anti-CXorf21/TASL (HPA001185), SLC38A9 (HPA043785, for IP) and anti-myc (C3956) from Sigma; anti-SLC15A4 (BMP055, for IP) and TLR8 (pd047) from MBL; anti-GAPDH (sc-365062), anti-I $\kappa$ B- $\alpha$  (sc-371), anti-LAMP2 (sc-18822), anti-HA (sc-805, for IP) and anti-STAT1 $\alpha$  (sc-417) from Santa Cruz; anti-Actin (AAN01-A) from Cytoskeleton, anti-Tubulin (ab7291), anti-IRF5 (ab181553) and anti-Lamp1 (ab25630) from Abcam. Custom rabbit anti-SLC15A4 antibodies raised against the N-terminus were generated with Genscript. Specificity was validated by western blot in SLC15A4 knockout and overexpressing cells (see Fig. 2a, Extended Data Figure 3g). Fluorescently labeled anti-PD-L1-APC (17-5983-42) was from Thermo Fisher Scientific, Alexa Fluor 488-coupled anti-mouse (A11001) and Alexa Fluor 594-coupled anti-rabbit (A11012) were from Life Technologies. Anti-HA and anti-V5 agarose beads were from Sigma, Protein G sepharose beads were from GE Healthcare. LysoTracker<sup>TM</sup> Red DND-99 and LysoSensor<sup>TM</sup> Green DND-189 were from Thermo Fisher Scientific. R848, CL075,

ssR40, ssR41, C12-iE-DAP, MDP, murabutide, ultrapure LPS (*E. coli* 0111:B4), Pam3CSK4, cGAMP, Flagellin from from *S. typhimurium*, unlabeled or FITC-labeled CpG-A (ODN2216), CpG-B (ODN2006) and BX795 were from Invivogen. TPCA-1 and PMA from Sigma. Recombinant human M-CSF, GM-CSF, IL-4, interferon  $\beta$ , and interferon  $\gamma$  were from Peprotech.  $\lambda$  phosphatase and PNGase F were from NEB.

## Cell culture

HEK293T cells and THP1 cells were purchased from ATCC, THP1 DUAL™ reporter cell lines from Invivogen. CAL-1 cells<sup>40</sup> were kindly provided by Prof. Takahiro Maeda, KBM-7 by Prof. Thijn Brummelkamp. Cells, except CAL-1, were authenticated by STR profiling and regularly tested for mycoplasma contamination. HEK293T cells were cultured in DMEM, THP1 in RPMI and KBM-7 cells in IMDM, supplemented with 10% (v/v) FBS and antibiotics (100 U/ml penicillin, 100 mg/ml streptomycin), all from Gibco. Cells were incubated at 37°C in 5% CO<sub>2</sub>. For differentiation of primary monocyte-derived macrophages and dendritic cells, CD14<sup>+</sup> monocytes were seeded in 6-well plates at a concentration of 1.5×10<sup>6</sup> cells in 2 ml per well RPMI medium supplemented with 10% (v/v) FBS and antibiotics (100 U/ml penicillin, 100 mg/ml streptomycin). Monocyte-derived macrophages were generated by stimulation for 1 week with 100 ng/ml M-CSF, dendritic cells by stimulation with 200 ng/ml GM-CSF and 50 ng/ml IL-4.

## Plasmids and siRNAs

CRISPR/Cas9-based knockout cell line generation was performed using pLentiCRISPRv2 (Addgene plasmid #52961). sgRNAs were designed using the Broad Institute sgRNA design tool (<https://portals.broadinstitute.org/gpp/public/analysis-tools/sgRNA-design>)<sup>47</sup>, the control sgRNA targeting *Renilla luciferase* (*sgRen*) was described previously<sup>48</sup>. Editing efficiencies for sgRNAs targeting *SLC15A2* and *SLC15A3* were determined by TIDE<sup>49</sup>. Cloned oligos were as follows (5' to 3' orientation):

sg*SLC15A2*-1, F: CACCGGATATAAAGGAATAGTACCC, R: AAACGGGTACTATTCCTTTATATCC;

sg*SLC15A2*-2, F: CACCGACTGAGCATTGCCTTCATTG, R: AAACCAATGAAGGCAATGCTCAGTC;

sg*SLC15A2*-3, F: CACCGAGGAGGCATCAAACCCTGTG, R: AAACCACAGGGTTTGATGCCTCCTC;

sg*SLC15A3*-1, F: CACCGGTTGGCGATGCCTCTTGCG, R: AAACCGCAAGAGGACATCGCCAACC;

sg*SLC15A3*-2, F: CACCGGAGAGCGAGCTTAAGCATAG, R: AAACCTATGCTTAAGCTCGCTCTCC;

sg*SLC15A3*-3, F: CACCGGCAGCGACAGCACAGCACCC, R: AAACGGGTGCTGTGCTGTGCTGCC;

sgSLC15A4-1, F: CACCGGGAGCGATCCTGTCGTTAGG, R:  
AAACCCTAACGACAGGATCGCTCCC;

sgSLC15A4-2, F: CACCGTATTACAACCACTCCTCACA, R:  
AAACTGTGAGGAGTGGTTGTAATAC;

sg *TASL-1*, F: CACCGGTAGAAATGGAATCCTCCAT, R:  
AAACATGGAGGATTCCATTTCTACC;

sg *TASL-2*, F: CACCGCTGAATTAATGGCCATCACC, R:  
AAACGGTGATGGCCATTAATTCAGC;

sg *IRF3-1*, F: CACCGGAGGTGACAGCCTTCTACCG, R:  
AAACCGGTAGAAGGCTGTCACCTCC;

sg *IRF3-2*, F: CACCGCCACTGGTGCATATGTTCCC, R:  
AAACGGGAACATATGCACCAGTGGC;

sg *IRF5-1*, F: CACCGAGGGCTTCAATGGGTCAACG, R:  
AAACCGTTGACCCATTGAAGCCCTC;

sg *IRF5-2*, F: CACCGATGAAGCCGATCCGGCCAAG, R:  
AAACCTTGCCGGATCGGCTTCATC;

sg *IRF7-1*, F: CACCGGATGCACTCACCTTGCACCG, R:  
AAACCGGTGCAAGGTGAGTGCATCC;

sg *IRF7-2*, F: CACCGGGCAGATCCAGTCCCAACCA, R:  
AAACTGGTTGGGACTGGATCTGCCC;

sg *TLR8*, F: CACCGACAGGAAGTTCCCCAAACGG, R:  
AAACCCGTTTGGGGAACCTCCTGTC;

sg *CHUK-1*, F: CACCGAAAGCTCCAATAATCAACAG, R:  
AAACCTGTTGATTATTGGAGCTTTC;

sg *CHUK-2*, F: CACCGTATACAGCTGCGTAAAGTGT, R:  
AAACACACTTTACGCAGCTGTATAC;

sg *CHUK-3*, F: CACCGTAGTTTAGTAGTAGAACCCA, R:  
AAACTGGGTTCTACTACTAACTAC;

sg *IKBKB-1*, F: CACCGCCATGGAGTACTGCCAAGG, R:  
AAACCCCTTGGCAGTACTCCATGGCC;

sg *IKBKB-2*, F: CACCGCAGCCATTGGGCCCATACGT, R:  
AAACACGTATGGGCCCAATGGCTGC;

sg *IKBKB-3*, F: CACCGTATTGACCTAGGATATGCCA, R:  
AAACTGGCATATCCTAGGTCAATAC;

sg*IKBKB-4*, F: CACCGGAAGCCCGTGATGCACTCAA, R:  
AAACTTGAGTGCATCACGGGCTTCC;

sg*IKBKE-1*, F: CACCGTCAACACTACCAGCTACCTG, R:  
AAACCAGGTAGCTGGTAGTGTGAC;

sg*IKBKE-2*, F: CACCGCGTGCACAAGCAGACCAGTG, R:  
AAACCACTGGTCTGCTTGTGCACGC;

sg*IKBKE-3*, F: CACCGATGATCTCCTTGTTCGCCG, R:  
AAACCGGCGGAACAAGGAGATCATC;

sg*IRAK4-1*, F: CACCGCTACGTAAATAACACAACCTG, R:  
AAACCAGTTGTGTTATTTACGTAGC;

sg*IRAK4-2*, F: CACCGGGCACCACAAATTGCACAGT, R:  
AAACACTGTGCAATTTGTGGTGCCC;

sg*IRAK4-3*, F: CACCGCATCTCATGTGCCAAGAAAG, R:  
AAACCTTTCTTGGCACATGAGATGC;

sg*IRAK4-4*, F: CACCGTGTAACATATACTAAGCAG, R:  
AAACCTGCTTAGTATATGTTTACAC;

sg*MAP3K7-1*, F: CACCGACCCAAAGCGCTAATTCACA, R:  
AAACTGTGAATTAGCGCTTTGGGTC;

sg*MAP3K7-2*, F: CACCGAATATTAGGATGGTTCACAC, R:  
AAACGTGTGAACCATCTAATATTC;

sg*MAP3K7-3*, F: CACCGCACACATGACCAATAACAAG, R:  
AAACCTTGTTATTGGTCATGTGTGC;

sg*TBK1-1*, F: CACCGTCCACGTTATGATTTAGACG, R:  
AAACCGTCTAAATCATAACGTGGAC;

sg*TBK1-2*, F: CACCGAATCAAGAAGCTTATCTACGA, R:  
AAACTCGTAGATAAGTTCTTGATTC;

sg*TBK1-3*, F: CACCGAAATATCATGCGTGTTATAG, R:  
AAACCTATAACACGCATGATATTC;

Codon-optimized cDNAs for human SLC15A3, human and murine SLC15A4, SLC15A3/SLC15A4 swap mutants, and human wildtype and scanning mutants of TASL were obtained from Genscript. A template for cloning of murine SLC15A3 was obtained from the Harvard Plasmid Repository (Clone ID: MmCD00319552), a template for cloning human TLR9 (pcDNA3-TLR9-YFP) was from (Addgene plasmid # 13642). cDNAs were subcloned to pDONR201 (Invitrogen) via Gateway cloning, Gateway donor plasmids for GFP and human SLC38A9 were described previously<sup>24</sup>. Deletion and point mutants were generated by PCR

or Q5 mutagenesis (NEB). All cDNAs were verified by sequencing and shuttled to Gateway destination vectors for untagged or N- or C-terminal Strep-HA (SH), V5 or myc-tagged expression. Rescue experiments were performed using codon-optimized cDNAs resistant to sgRNAs targeting endogenous genes. For lentiviral transduction, cDNAs were shuttled to pRRL-based lentiviral expression plasmids and a selectable resistance cassette described previously<sup>48</sup>. Lentiviral packaging plasmids psPAX2 (Plasmid #12260) and pMD2.G (Plasmid #12259) were obtained from Addgene. Non-targeting control and human *SLC15A4*, *TASL* and *MYD88*-specific ON-TARGETplus SMARTpool siRNAs were obtained from Dharmacon. Non-targeting pool, siCTRL (Cat.: D-001810-10-05): siRNA #1: 5'-UGGUUUACAUGUCGACUAA-3', siRNA #2: 5'-UGGUUUACAUGUUGUGUGA-3', siRNA #3: 5'-UGGUUUACAUGUUUCUGA-3', siRNA #4: 5'-UGGUUUACAUGUUUCCUA-3'). Human *SLC15A4* (Cat.: L-007401-02-0005): siRNA #1: 5'-CGACCAGGUUAAAGAUCGA-3', siRNA #2: 5'-GAAGCGAAGUGGAGAGCGC-3', siRNA #3: 5'-CCUGAGGCCAUGUGCGGUU-3', siRNA #4: 5'-GCAUUAACCUUGGAGCGAU-3'). Human *TASL/CXorf21* (Cat.: L-014600-02-0005): siRNA #1: 5'-GCAGAAGGUUGUGGAGUUA-3', siRNA #2: 5'-CAAUGUAAAUCAUAGAGA-3', siRNA #3: 5'-GGACUUGAGUACUGGAAUG-3', siRNA #4: 5'-CCAUUAUUCAGUGACAAC-3'). Human *MYD88* (Cat.: L-004769-00-0005): siRNA #1: 5'-CGACUGAAGUUGUGUGUGU-3', siRNA #2: 5'-GCUAGUGAGCUCAUCGAAA-3', siRNA #3: 5'-GCAUAUGCCUGAGCGUUUC-3', siRNA #4: 5'-GCACCUUGUGUCUGGUCUAU-3').

### Lentiviral gene transduction

For lentiviral gene transduction, HEK293T cells transfected with the respective lentiviral vectors and packaging plasmids psPAX2 and pMD2.G using Polyfect (QIAGEN) or PEI. 24h later, medium was exchanged to RPMI, supplemented with 10% (v/v) FBS and antibiotics (100 U/ml penicillin, 100 mg/ml streptomycin). 48h after transfection, cell supernatants were harvested, filtered through 0.45 µm polyethersulfone filters (GE Healthcare) and supplemented with 8 µg/ml protamine sulfate (Sigma). Cells were infected by spinfection (2000 rpm, 45 minutes, room temperature). 24h after infection, medium was changed, 48h after infection, cells were selected with the respective antibiotics.

### Cell lysis, western blotting and co-immunoprecipitation

Cells were lysed in RIPA (25 mM Tris, 150 mM NaCl, 0.5% NP-40, 0.5% deoxycholate (w/v) and 0.1% SDS (w/v), pH 7.4) or E1A (50 mM HEPES, 250 mM NaCl, 5 mM EDTA, 1% NP-40, pH 7.4) lysis buffer supplemented with Roche EDTA-free protease inhibitor cocktail (1 tablet/50 ml) for 10 min on ice. Where phospho-proteins were analyzed, lysis buffer was supplemented with Halt phosphatase inhibitor cocktail (Thermo Fisher Scientific). Lysates were cleared by centrifugation at 13000 rpm, 10 min, 4°C and normalized by Bradford protein assay (Bio-Rad) or BCA (Thermo Fisher Scientific) using BSA as standard. Typically, 20 µg protein per sample was resolved by regular or 20 µM Phos-tag-containing (WAKO Chemicals) SDS-PAGE and blotted to nitrocellulose membranes. Membranes were blocked with 5% non-fat dry milk in TBST and probed with the indicated antibodies. Binding was detected with horseradish peroxidase--conjugated secondary antibodies using the ECL Western blotting system (Thermo Fisher Scientific). In

figures where multiple antibodies were used, equal amounts of samples were loaded on multiple SDS-PAGE gels and western blots sequentially probed with a maximum of two antibodies. For immunoprecipitation experiments of overexpressed proteins, cells were lysed in E1A buffer. Whole cell lysate was removed as input, the rest subjected to immunoprecipitation using equilibrated anti-HA or V5 agarose beads (Sigma) over night at 4°C. Beads were washed three times with E1A buffer and eluted with SDS sample buffer. In experiments monitoring co-immunoprecipitation of IRF5, the second wash step was performed with E1A buffer containing higher NaCl concentration (500 mM). Samples were analyzed by western blot as described above. For immunoprecipitation of endogenous proteins,  $1.5 \times 10^7$  cells per condition were lysed in 500  $\mu$ l E1A buffer. 40  $\mu$ l whole cell lysate was removed as input, the rest subjected first to a pre-clearing step on Sepharose 6 beads (Sigma) (40 min with rotation, 4°C) and then to immunoprecipitation using 20  $\mu$ l equilibrated protein G-sepharose (GE healthcare) and primary antibody (SLC15A4 BMP055 MBL; SLC38A9 HPA043785 Sigma; HA sc-805 Santa Cruz) (over night with rotation, 4°C). Beads were washed three times with E1A buffer and eluted with 60  $\mu$ l SDS sample buffer.

### **PNGase F treatment**

Cells were lysed in E1A buffer. Per sample, 20  $\mu$ l cleared lysate was either incubated without or with 1-2  $\mu$ l (500-1000u) PNGase F (NEB) for 30 minutes at 37°C. Samples were analyzed by western blotting.

### **$\lambda$ phosphatase treatment**

Immunoprecipitates were generated as described above. Washed beads were resuspended in 60  $\mu$ l NEB PMP buffer + 1 mM  $MnCl_2$ , split in two and incubated or not with 1  $\mu$ l (400u)  $\lambda$  phosphatase (NEB) for 30 minutes at 30°C. Samples were analyzed by western blot.

### **ELISA**

All ELISA experiments were carried out using diluted cell culture supernatants according to the manufacturer's instructions. ELISA kits for human TNF (#88-7346-88) and IL-8 (#88-8086-88) were from Invitrogen, human IL-6 (#88-7066-88) from eBioscience; ELISA kits for human CCL2 (#DY279) and CCL5 (#DY278) were from R&D Systems, for human interferon  $\beta$  from PBL Assay Science (41410-1).

### **THP1 DUAL cells reporter assay**

THP1 DUAL cells ( $1 \times 10^5$  cells per 96 well) were stimulated as indicated for 20-24 hours. Cell culture supernatants were harvested, cleared of residual cells by centrifugation and analyzed for NF- $\kappa$ B and ISRE reporter activity according to the manufacturer's instructions.

### **Flow cytometry**

For PD-L1, cells were stained with APC-conjugated anti-PD-L1 antibodies (17-5983-42, Thermo Fisher Scientific) according to the manufacturer's instructions. For uptake assays of FITC-labeled CpG, cells were incubated with 1  $\mu$ M CpG-A (ODN2216) or CpG-B (ODN2006) for 0-120 minutes. Cells were washed with PBS and analyzed immediately by

flow cytometry. Data was acquired on a BD FACSCalibur (BD Biosciences) and analyzed using FlowJo software (version 10).

### Confocal microscopy

For staining of fixed cells,  $1 \times 10^5$  cells were seeded in 24-well plates on cover slips and treated with 10 nM PMA over night to induce adherence. Cells were fixed for ten minutes with 4% formaldehyde in PBS and permeabilized and blocked with 0.3% saponin (Sigma) and 10% FBS in PBS for 1h. Cells were stained overnight at 4°C with the indicated primary antibodies (rabbit anti-HA: 1:400, mouse anti-Lamp1: 1:200) in blocking solution. Cells were washed three times in blocking solution and stained for 1h with fluorescently labeled anti-rabbit and anti-mouse secondary antibodies (1:400) at room temperature. Cells were washed three times in blocking solution and once in PBS. Nuclear counterstaining was performed with DAPI (Thermo Fisher Scientific), diluted 1:1000 in PBS and cover glasses were mounted onto microscope slides using ProLong Gold (Thermo Fisher Scientific) antifade reagent. For live cell imaging of TASL-GFP expressing THP1 cells, cells were stained with LysoTracker™ Red DND-99 (1:10000) and Hoechst 33342 (1:1000, Thermo Fisher Scientific) for 30 minutes and washed with PBS. Images were acquired on a confocal laser scanning microscope (Zeiss LSM 780, Carl Zeiss AG, Germany) and analyzed using ZEN 2.3 (Carl Zeiss AG).

### siRNA knockdown in human primary monocytes

PBMCs from healthy donors were obtained by density gradient centrifugation of buffy coat material obtained from the Austrian Red Cross with Lymphoprep (Stem Cell Technologies). CD14<sup>+</sup> monocytes were purified from PBMCs using CD14-specific MACS immunomagnetic beads (Miltenyi) according to the manufacturer's instructions. siRNAs were transfected according to a modified protocol previously described<sup>50</sup>. Lipid-siRNA complexes were prepared by combining 15 µl siRNA (20 µM stock) with 470 µl non-supplemented RPMI medium and addition of 15 µl HiPerfect transfection reagent (QIAGEN). After 15-20 minutes, complexes were transferred to 6-well plates and combined with  $1.5 \times 10^6$  monocytes/well in 1 ml RPMI medium supplemented with 10% (v/v) FBS and antibiotics (100 U/ml penicillin, 100 mg/ml streptomycin). Next day, 1 ml supplemented RPMI medium was added to each well. Stimulation experiments and RNA isolation for analysis of knockdown efficiency were carried out 48h after transfection. Cell supernatants were analyzed for TNF secretion by ELISA. Based on the seven donors, the following differences were tested employing a paired t-test (two-sided) on the log<sub>2</sub>-transformed TNF concentrations, assuming normality: si*SLC15A4* vs. siCTRL (effect size: -0.69; 95% confidence interval: [-1.31, -0.07]; t-statistic: -2.72; p-value: 0.035; degrees of freedom: 6), si*TASL* vs. siCTRL (effect size: -1.97; 95% confidence interval: [-2.63, -1.30]; t-statistic: -7.19; p-value:  $3.66 \times 10^{-4}$ ; degrees of freedom: 6), and si*MYD88* vs. siCTRL (effect size: -0.90; 95% confidence interval: [-1.73, -0.07]; t-statistic: -2.65; p-value: 0.038; degrees of freedom: 6).

### RealTime PCR

RNA from monocytes was isolated 48h after siRNA transfection using the QIAGEN RNeasy Mini kit including DNase I digestion step. The reverse transcription was performed using

RevertAid First Strand cDNA Synthesis Kit (Thermo Scientific) using oligo dT primers, RealTime-PCR was performed using the SensiFAST™ SYBR® Hi-ROX kit (Bioline) according to the manufacturer's instructions. The primers used are: *GAPDH*F: 5'-CCTGACCTGCCGTCTAGAAA-3', R: 5'-CTCCGACGCCTGCTTAC-3'; *SLC15A4*F: 5'-CGGATGGATGAGCAGTCACA-3', R: 5'-AGGAAAAGCAGGAGGGTAGC-3'; *TASL*F: 5'-GGAAAGAGCATTGGCTGGCTT-3', R: 5'-TTCTCACTGACCTTCACTAACCA-3'; *MYD88*F: 5'-GAGCTCATCGAAAAGAGGTGC-3', R: 5'-GGAGAGAGGCTGAGTGCAAA-3'. Samples were analyzed on a LightCycler 480 (Roche) or Rotor Gene Q (QIAGEN). Amplification on LightCycler 480 consisted of an initial incubation at 95 °C for 10 min, followed by 40 cycles of 95 °C for 5 s, 60 °C for 60 s and 72 °C for 6 s and a final cooling to 40 °C. Data was analyzed and Ct was calculated using LightCycler Software Version 1.5 (Roche). Amplification on Rotor Gene Q consisted of an initial incubation at 95 °C for 10 min, followed by 40 cycles of 94 °C for 30 s, 60 °C for 15 s and 72 °C for 30 s and a final cooling to 25 °C. Data was analyzed and Ct was calculated using the Rotor Gene Series Software Version 2.2.2 (QIAGEN). Results were obtained using the  $2^{-C(t)}$  method, using *GAPDH* as reference.

### Affinity purification and mass spectrometry

Affinity purifications and sample preparation for liquid chromatography mass spectrometry (LC-MS/MS) were performed as previously described<sup>24,51,52</sup>. Two affinity purifications were performed as biological replicates and cell lines expressing Strep-HA-tagged GFP were used as negative controls. LC-MS/MS was performed on the following instruments: Hybrid linear trap quadrupole (LTQ) Orbitrap Velos, Q Exactive™ or Orbitrap Fusion™ Lumos™ Tribrid™ mass spectrometer (Thermo Fisher Scientific, San Jose, CA) coupled to either an Agilent 1200 (Agilent Biotechnologies, Palo Alto, CA) or Dionex U3000RSLC U/HPLC nanoflow system (Thermo Fisher Scientific, San Jose, CA) via Nanospray Flex™ Ion source interface. Tryptic peptides were loaded onto a trap column using 0.1% TFA as loading buffer. After loading, the trap column was switched in-line with a 75 µm inner diameter analytical column (packed in-house with ReproSil-Pur 120 C18-AQ, 3 µm, Dr. Maisch, Ammerbuch-Entringen, Germany). Mobile-phase A consisted of 0.4% formic acid in water and mobile-phase B of 0.4% formic acid in a mix of 90% acetonitrile and 9.6% water. The flow rate was set to 230 nL/min and either a 30 min (3 to 36% solvent B within 30 min) or a 90 min (4 to 30% solvent B within 81 min, 30 to 65% solvent B within 8 min and, 65 to 100% solvent B within 1 min) gradient was applied, followed by flushing at 100% solvent B for 6 min before re-equilibration of the column material at 3% solvent B for 18 min prior to next injection. MS instruments were operated in data-dependent acquisition (DDA) mode with top 10 or 15 most intense precursor ions selected for collision-induced dissociation (CID) in the linear ion trap (LTQ) or higher energy collision induced dissociation in the HCD cell. MS<sup>1</sup>-spectra were acquired in the Orbitrap mass analyzer at high resolution, while MS<sup>2</sup>-fragment ion spectra were acquired either in the linear ion trap at low resolution (Velos) or in the Orbitrap at high resolution (Q Exactive or Fusion Lumos). Automatic gain control was used to control the number of ions accumulated in the respective ion traps. A single lock mass at m/z 445.120024 was employed<sup>53</sup>. All samples were analyzed in technical duplicates.

## MS data analysis

For the TAP-MS experiments (Fig. 1b,e), MS2 spectra generated from +2, +3 or +4 charged precursor ions were extracted from the raw output files using msconvert from the ProteoWizard library (version 3.0.11220)<sup>54</sup>. A protein search database was compiled based on the UniProt Homo sapiens reference proteome (release 2017\_07; 71,591 entries)<sup>55</sup>, extended by 248 typical contaminant sequences from MaxQuant (version 1.6.0.13)<sup>56</sup> and concatenated with reversed and shuffled decoy sequences generated by DecoyPYrat<sup>57</sup>. Spectra were matched to semi-tryptic peptides of 6-40 amino acids of this database using MS-GF+ (version 2017.01.13)<sup>58</sup> allowing for a precursor mass error of up to 20ppm and an isotope error of -1 to +2. All cysteines were considered carbamidomethylated and methionines optionally oxidated. Generated peptide-spectrum matches (PSMs) were post-processed based on the target-decoy approach<sup>59</sup> using Percolator (version 3.01)<sup>60</sup> and filtered for an estimated FDR of less than 1%. Protein groups implied by peptides across all samples was simplified using an in-house script based on Occam's razor principle. The number of PSMs per gene (based on UniProt annotation) and biological sample (collapsing technical replicates) served as input to SAINT (version 2)<sup>61</sup> for probabilistic scoring of bait-prey interactions using the GFP samples as control. Significant interactions (FDR of less than 1%) were visualized as network in Cytoscape 3.5.1<sup>62</sup>. The network was filtered to exclude non-specific interactors showing an average spectral count of 10 or more in the 411 control samples of the CRAPome database (version 1.1)<sup>63</sup>. For the IP-MS experiments (Fig. 4g, Extended Data Fig. 9g), acquired raw data files were processed using the Proteome Discoverer 2.2.0.388 platform, utilising the database search engine Sequest HT. Percolator V3.0 was used to remove false positives with a false discovery rate (FDR) of 1% on peptide and protein level under strict conditions. Searches were performed with full tryptic digestion against the human SwissProt database v2017.06 (20,456 sequences and appended known contaminants) with up to two miscleavage sites. Oxidation (+15.9949 Da) of methionine was set as variable modification, whilst carbamidomethylation (+57.0214 Da) of cysteine residues was set as fixed modifications. Data was searched with mass tolerances of  $\pm 10$  ppm and 0.025 Da on the precursor and fragment ions, respectively. Results were filtered to include peptide spectrum matches (PSMs) with Sequest HT cross-correlation factor (Xcorr) scores of 1 and high peptide confidence. For Fig. 4g, obtained protein abundances by the Proteome Discoverer software were normalized for each sample to the corresponding mean bait abundance. Based on three biological replicate measurements, the following differences were tested employing Welch's t-test (two-sided) on the normalized, log<sub>2</sub>-transformed abundances, assuming normality but unequal variances. In the wild type, IRF5 abundance increases significantly upon CpG induction (effect size: +3.48; 95% confidence interval: [+3.03, +3.94]; t-statistic: 24.97; p-value:  $2.09 \times 10^{-4}$ ; degrees of freedom: 2.83). CpG induced abundance of IRF5 is significantly lower in wild type compared to the point-mutant (effect size: -2.20; 95% confidence interval: [-2.57, -1.82]; t-statistic: -18.16; p-value:  $2.77 \times 10^{-4}$ ; degrees of freedom: 3.14).

## Multiple sequence alignment and secondary structure prediction

Protein sequences were extracted from the UniProt<sup>64</sup> database and aligned with ClustalX2.1<sup>65</sup> using default settings. Secondary structure prediction was performed for the human TASL sequence using JPred4<sup>66</sup>.

### Gene expression analysis (RNA-Seq)

THP1 control (*sgRen*) and two knockout cell lines per gene ( $3 \times 10^6$  cells per point) were left untreated or stimulated for six hours with 5  $\mu\text{g/ml}$  R848 or 2  $\mu\text{M}$  CpG-B (ODN2006). Cells were harvested and RNA was isolated using the QIAGEN RNeasy Mini kit including a DNase I digest step. RNA-Seq libraries were prepared using QuantSeq 3' mRNA-Seq Library Prep Kit FWD for Illumina (Lexogen) according to the manufacture's protocol. Libraries were subjected to 50-bp single-end high-throughput sequencing on an Illumina HiSeq 4000 platform at the Biomedical Sequencing Facility (<https://biomedical-sequencing.at/>). Raw sequencing reads were demultiplexed, and after barcode, adaptor and quality trimming with cutadapt (<https://cutadapt.readthedocs.io/en/stable/>), quality control was performed using FastQC (<http://www.bioinformatics.babraham.ac.uk/projects/fastqc/>). The remaining reads were mapped to the GRCh38/h38 human genome assembly using genomic short-read RNA-Seq aligner STAR version 2.5<sup>67</sup>. We obtained more than 98 % mapped reads in each sample with 70 – 80 % of reads mapping to unique genomic location. Transcripts were quantified using End Sequence Analysis Toolkit (ESAT)<sup>68</sup>. Differential expression analysis was performed using three biological replicates with DESeq2 (1.21.21) on the basis of read counts<sup>69</sup>. Exploratory data analysis and visualizations were performed in R-project version 3.4.2 (Foundation for Statistical Computing, Vienna, Austria, <https://www.R-project.org/>) with Rstudio IDE version 1.0.143, ggplot2 (3.0.0), dplyr (0.7.6), readr (1.1.1), gplots (3.0.1).

### Transcription factor targets enrichment test

Tissue and cell-type specific high-level regulatory networks were extracted from Network compendium - regulatorycircuits.org<sup>70</sup>. Network was filtered to extract strong transcription factor to target associations. Enrichment was analyzed using Fisher's exact test and p-values were corrected for multiple testing using FDR procedure<sup>71</sup>. Background and gene sets are described in the corresponding figure legends.

### Gene ontology enrichment analysis

Gene ontology (GO) biological process enrichment analysis for genes was performed using the Database for Annotation, Visualization and Integrated Discovery (DAVID) functional annotation tool, version 6.8<sup>72</sup>. Background and gene sets are described in the corresponding figure legends.

### Expression database analysis of SLC15A4 and TASL

RNA-Seq data for cancer cell lines were obtained from<sup>29</sup> and grouped into tissues using the original annotation provided. CAGE data for primary cells were downloaded as of April 2017 from the FANTOM5 website ([fantom.gsc.riken.jp/5/](http://fantom.gsc.riken.jp/5/))<sup>30</sup>. Only TPM values for p1 peaks were considered for each gene. Cell types were manually annotated to their corresponding tissues. Plotting was done using R.

### Molecular docking

The TASL phosphomimetic *p*LxIS-containing peptide (residues 286-299, ISTPSLHIDQYSNV) was docked on the structure of IRF5 (PDB ID 3DSH) using CABS-

dock<sup>73</sup>. A constraint was applied to anchor the phosphomimetic residue to the IRF5 residue Arg353 based on the similarity between the IRF5 structure and IRF3 bound to STING/MAVS/TRIF pLxIS-containing peptides<sup>11</sup>. The top solution was further refined with the FlexPepDock algorithm<sup>74</sup> and the top ranking model compared to the structures of IRF3/peptide complexes.

### Phagocytosis assay

Phagocytosis assays were carried out as previously described<sup>75</sup>. Fluoresbrite carboxylated 1.75  $\mu\text{M}$  microspheres (Yellow Green: 441 nm excitation, 486 nm emission, Polyscience, Cat#17687-5) were opsonized in 50% human male AB serum in PBS for 16 hours at 4°C under constant rotation. Beads were then washed twice with PBS and labeled with 2  $\mu\text{g}/\text{mL}$  pHrodo-Red, SE (Thermo Fisher Scientific, Cat#P36600) for 30 min at room temperature with agitation. Next beads were washed once with PBS and were resuspended afterwards to a final concentration of  $1 \times 10^9$  beads/mL.

THP1 cells were PMA differentiated and seeded on 12-well cell culture coated dishes ( $1 \times 10^6$  cells/well). Labeled beads were then added at an MOI of 10 and incubated with the cells for 3 hours. Subsequently, cells were washed three times with ice-cold PBS and afterwards detached by scraping with a cell scraper (Sarstedt) and analyzed by flow cytometry. For the Bafilomycin A1 (Enzo) control assay, the compound was added to the cell culture medium 30 min before addition of the labeled beads and added to the cell culture medium during the entire assay at a final concentration of 200 nM.

On flow cytometry, the intensity of the pH-insensitive dye (YG) and the intensity of pHrodo-Red, which reacts with an increase in signal to decreasing pH, were recorded. Cells that did not take up the labeled beads are negative for both signals and considered incapable of phagocytosis (PhagoNeg). Cells positive for the YG and a high pHrodo-Red signal underwent phagocytosis and phagosome acidification (PhagoLate). Cells only positive for YG signal and with a low pHrodo-Red signal, are in an early stage of phagocytosis (PhagoEarly).

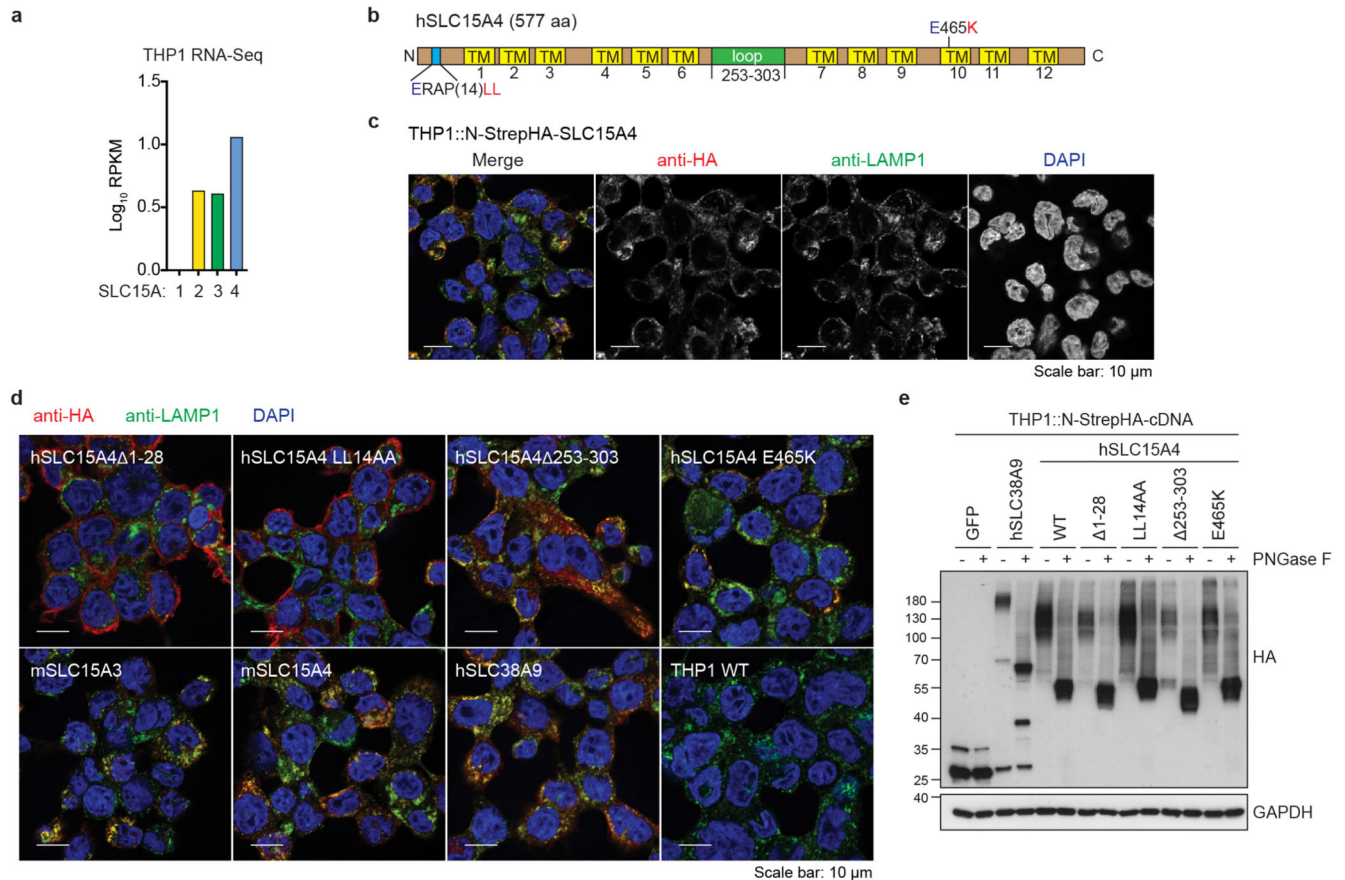
Flow cytometry data acquisition was conducted on an LSR Fortessa II cytometer interfaced with FACSDiva (BD) and analyzed using FlowJo software (v. 10).

### Quantification of LysoSensor™ intensities

For the imaging-based quantification of LysoSensor™ Green DND-189 (Thermo Fisher Scientific) in lysosomal compartments,  $1 \times 10^5$  cells were co-stained with LysoSensor™ Green (1:1000), LysoTracker™ Red DND-99 (1:10000) (Thermo Fisher Scientific) and Hoechst 33342 (1:1000) (Thermo Fisher Scientific) for 30 minutes in normal growth conditions. After pelleting by centrifugation, cells were resuspended in growth medium supplemented with 25  $\mu\text{M}$  HEPES and transferred onto CellCarrier-384 Ultra Microplates (PerkinElmer Inc., USA). Following a brief centrifugation, cells were imaged on an Opera Phenix High-Content screening System (PerkinElmer) in confocal mode using the 63 $\times$  water immersion objective. Image analysis and lysosomal LysoSensor™ quantification were performed in CellProfiler version 3.1.5<sup>76</sup> and R version 3.4.4 (see Fig. EV11B for flow diagram). In brief, Hoechst 33342 and LysoSensor™ stainings were used for the detection of

nuclei and cells. In a consecutive step, the LysoTracker™ signal allowed for the identification of lysosomes within cells and LysoSensor™ intensities were quantified within the identified lysosomal compartments. Plotting of the acquired data for visual representation was performed in R.

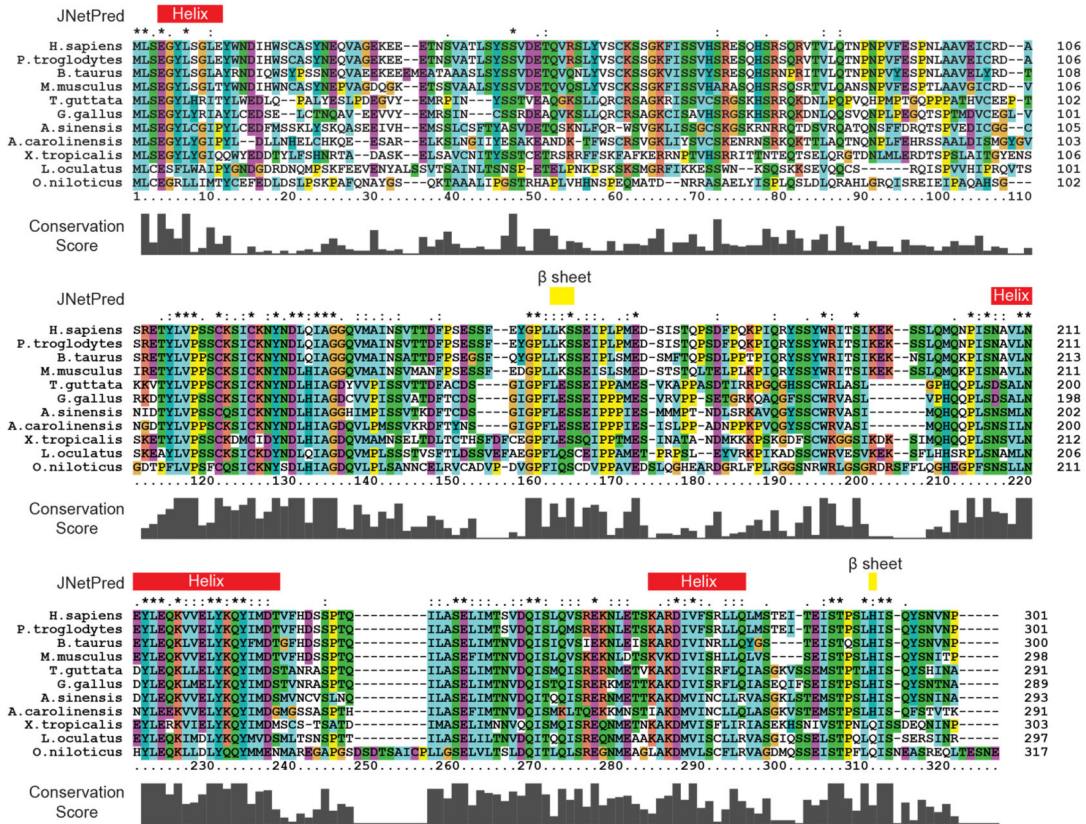
## Extended Data



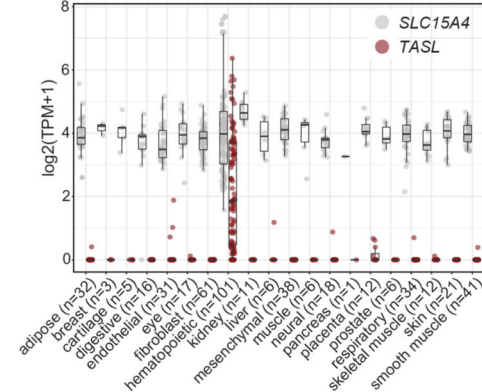
### Extended Data Figure 1. Subcellular localization of tagged SLC15A4 and related constructs in THP1 cells.

(a) Gene expression levels of SLC15A1-4 in THP1 cells from<sup>29</sup> (b) Domain organization of SLC15A4 protein. TM: transmembrane domain. (c,d) Confocal microscopy of indicated THP1 cells. Red: anti-HA, green: anti-Lamp1, blue: DAPI. Scale bar: 10 μm. (e) Lysates from indicated THP1 cells untreated or treated with PNGase F were analyzed by immunoblotting. (c-e) Data representative of two independent experiments. For gel source data, see Supplementary Figure 1.

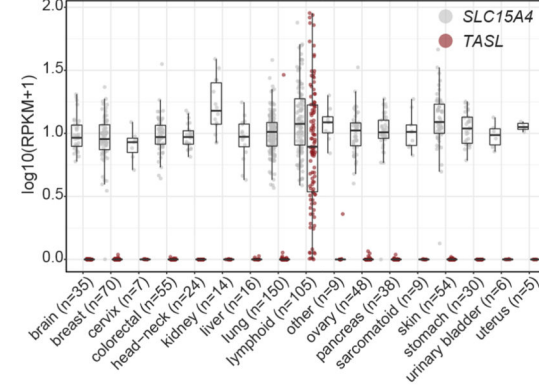
**a** Multiple sequence alignment for TASL



**b** Gene expression (FANTOM5, CAGE)

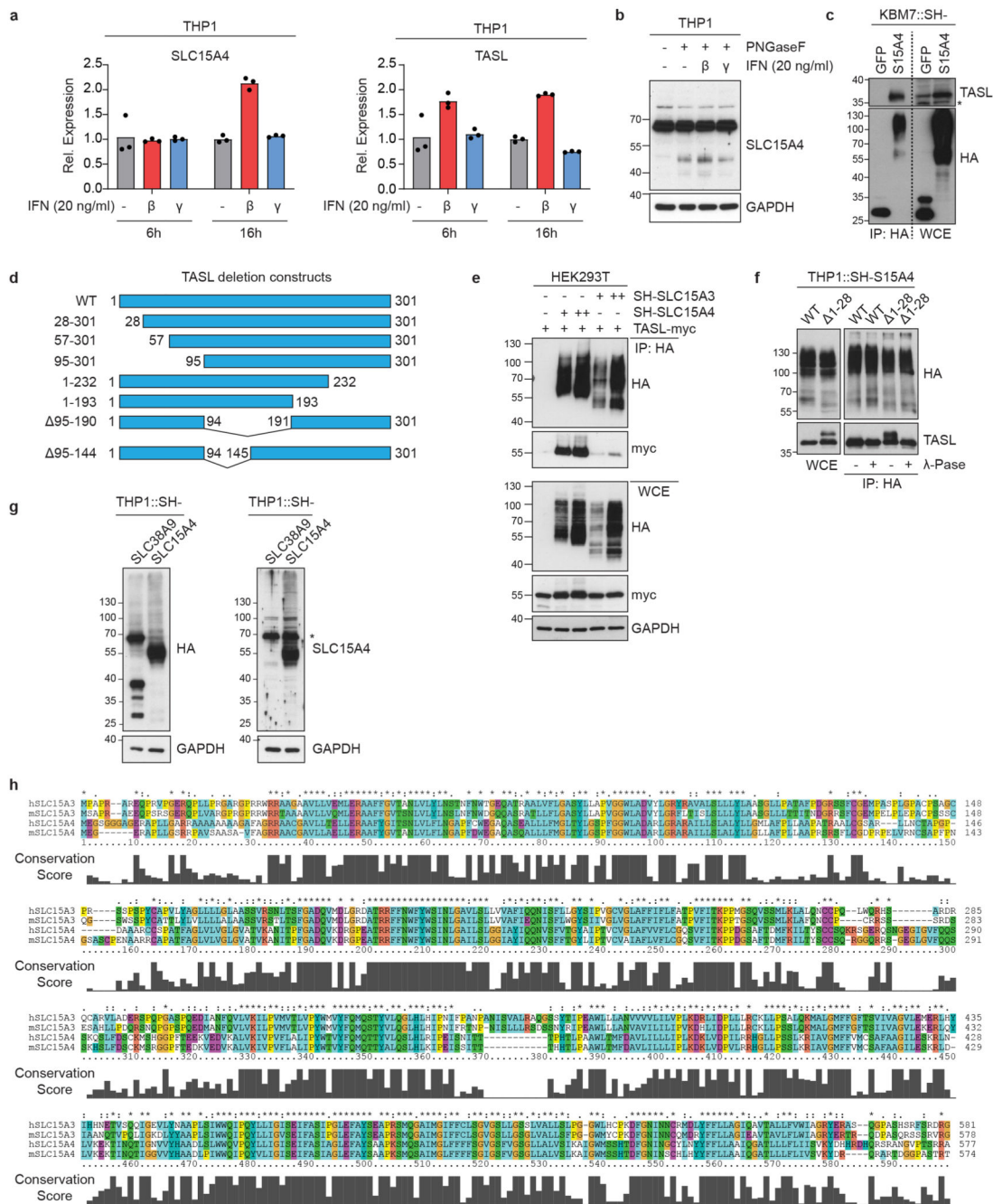


**c** Gene expression (Klijn et al., RNA-Seq)



**Extended Data Figure 2. TASL is an immune cell-restricted protein conserved in vertebrates.**  
**(a)** Multiple sequence alignment of TASL protein from representative vertebrate species. UniProt entry names: CX021\_HUMAN, H2QYF9\_PANTR, CX021\_BOVIN, CX021\_MOUSE, H0Z9M3\_TAEGU, A0A1L1RS25\_CHICK, A0A1U7RX84\_ALLSI, G1KG99\_ANOCA, F7BWY0\_XENTR, W5NMP6\_LEPOC, I3KXE0\_ORENI. Boxes above the alignment indicate consensus prediction from JPred4. Red: helix, yellow:  $\beta$  sheet.  
**(b, c)** Expression levels of *SLC15A4* and *TASL* in **(b)** primary human cells as measured by CAGE by FANTOM5<sup>30</sup> and in **(c)** human cancer cell lines measured by RNA-Seq from<sup>29</sup>.

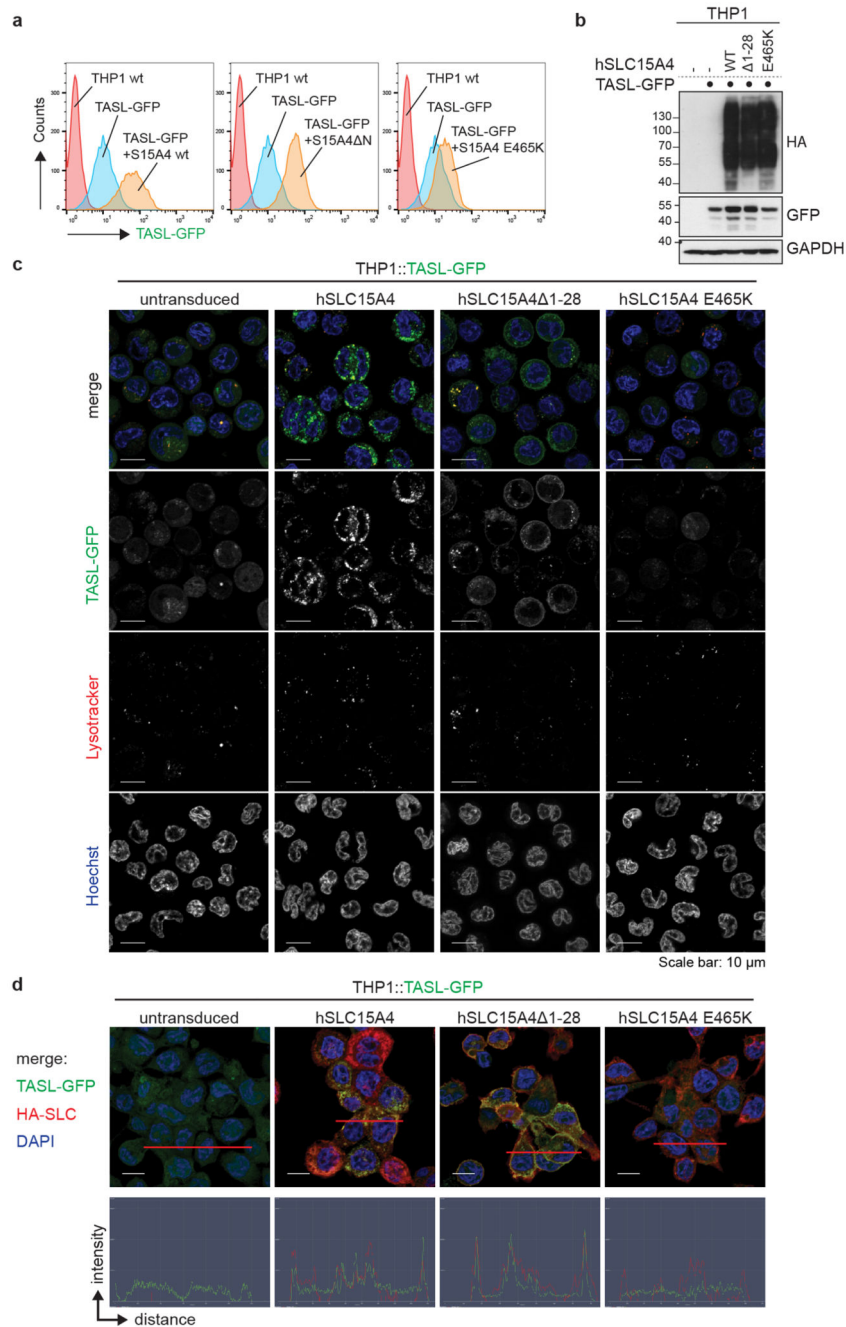
Circles represent individual samples, in boxplots, bars indicate median, boxes the first–third quartiles. Upper whisker extends from hinge to largest value no further than 1.5 \* IQR (inter-quartile range) from the hinge. Lower from hinge to smallest value at most 1.5 \* IQR of the hinge.



**Extended Data Figure 3. Type I interferon-inducible TASL forms a complex with SLC15A4.**

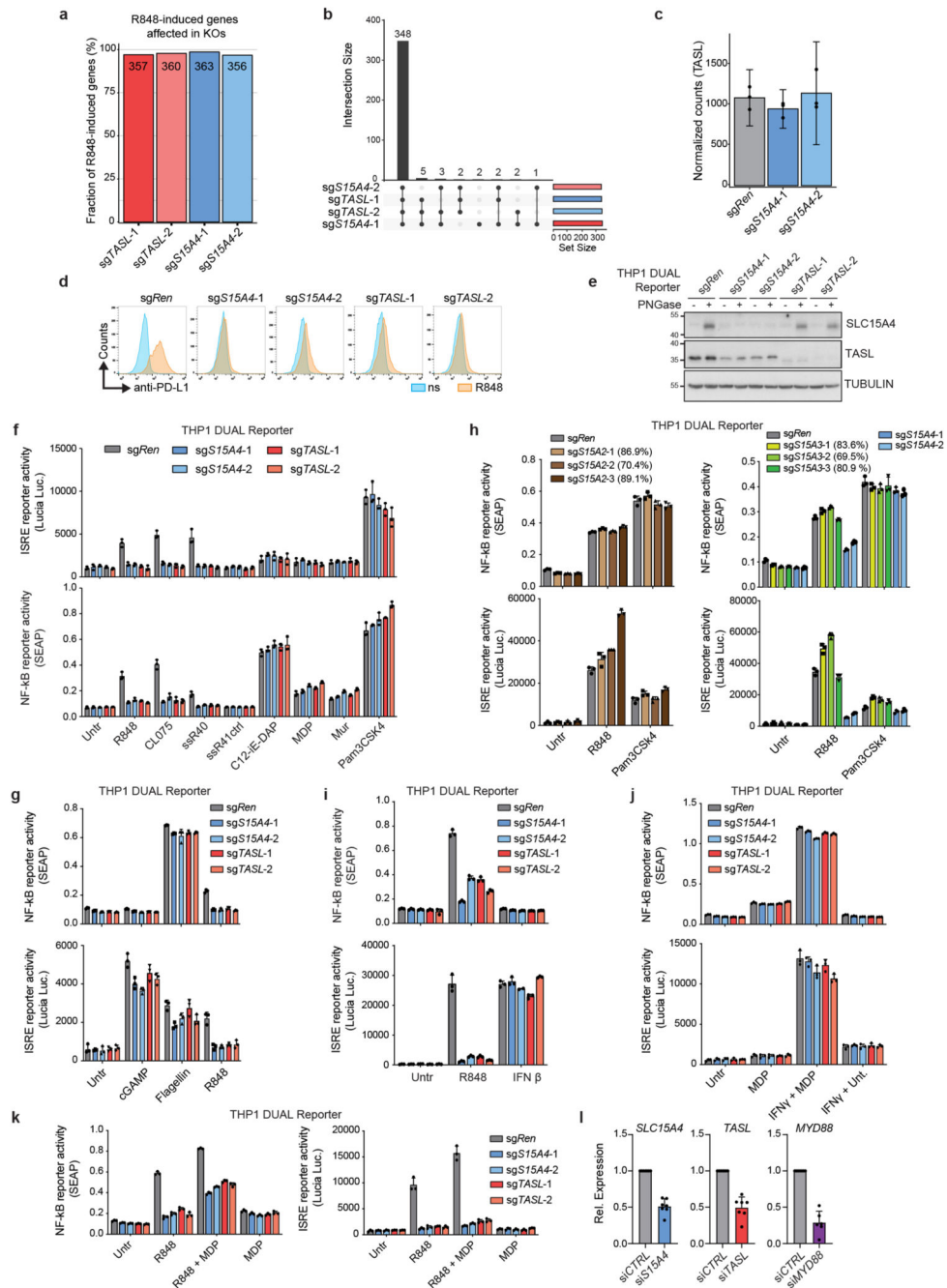
(a) Normalized mRNA expression of *SLC15A4* and *TASL* relative to *GAPDH* in THP1 cells treated as indicated. Data show mean (n=3 technical replicates). (b) Immunoblots of lysates

of THP1 cells stimulated with interferon  $\beta$  or  $\gamma$  (20 ng/ml, 16h) treated with PNGase F as indicated. **(c,e)** Lysates from **(c)** KBM7 cells transduced or **(e)** HEK293T cells transiently transfected as indicated were subjected to HA-immunoprecipitation. Immunoprecipitates (IP) and whole cell extracts (WCE) were analyzed by immunoblotting. **(d)** Overview of deletion mutants used in Fig. 1g. **(f)** Lysates from indicated THP1 cells were subjected to HA-immunoprecipitation and treated or not with  $\lambda$  phosphatase. IP and WCE were analyzed by immunoblotting. **(g)** Immunoblots of indicated THP1 cells treated with PNGase F. **(h)** Multiple sequence alignment of human and murine SLC15A3 and SLC15A4. UniProt entry names: S15A3\_HUMAN, S15A3\_MOUSE, S15A4\_HUMAN, S15A4\_MOUSE. **(a-c,e-g)** Data representative of two independent experiments. For gel source data, see Supplementary Figure 1.



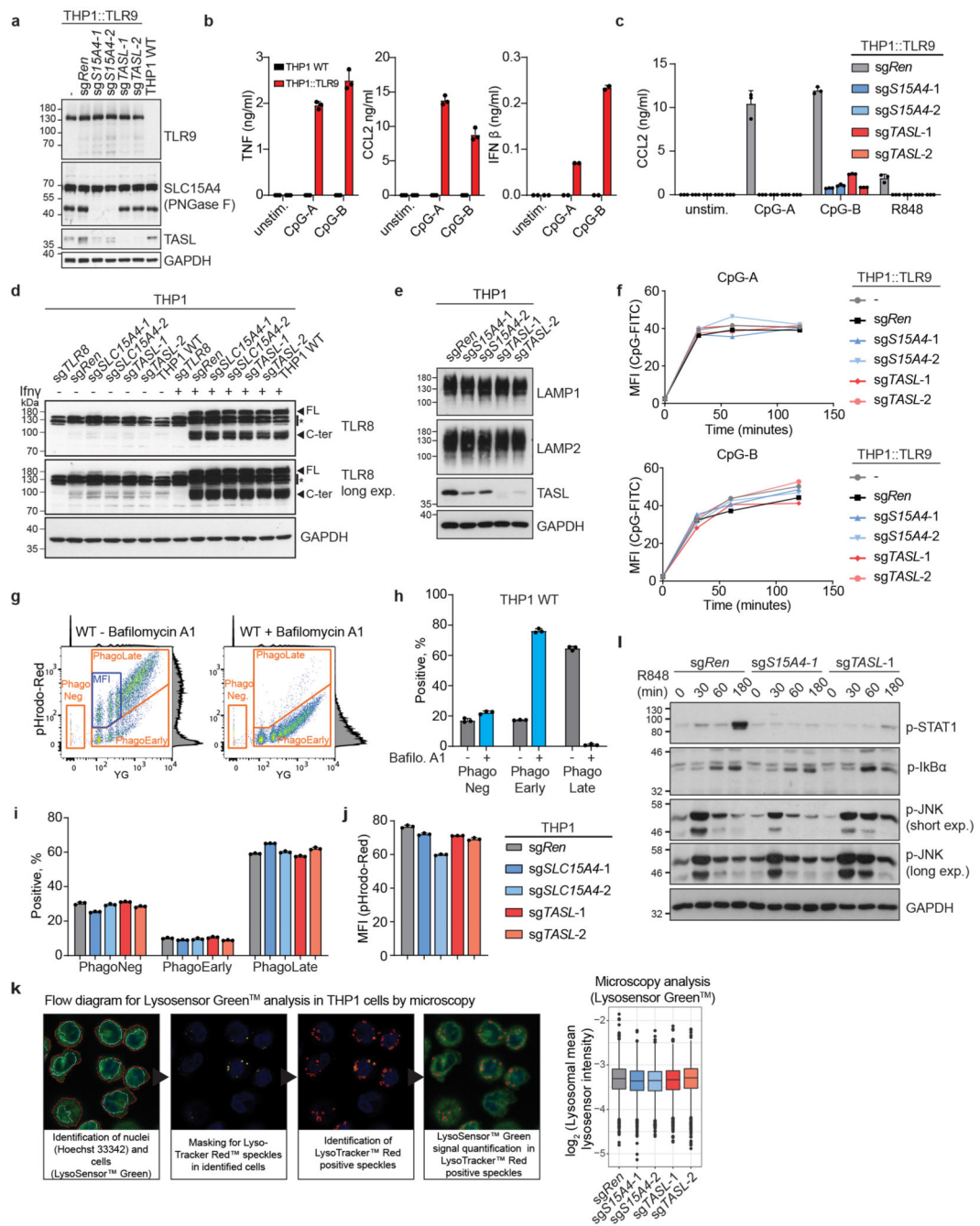
**Extended Data Figure 4. SLC15A4 controls TASL protein abundance and subcellular localization.**

**(a,b)** **(a)** Flow cytometry and **(b)** immunoblot of indicated THP1 cells. **(c)** Confocal live microscopy of indicated THP1 cells. Green: TASL-GFP, Red: Lysotracker, Blue: Hoechst33342. Scale bar: 10 μm. **(d)** Upper panel: Confocal microscopy of indicated formaldehyde-fixed THP1 cells. Green: TASL-GFP, Red: HA, Blue: DAPI. Scale bar: 10 μm. Lower panel: profiles of signal intensity of TASL-GFP (green) and HA (red) along the red lines shown in microscopy images (upper panel). **(a-d)** Data representative of two independent experiments. For gel source data, see Supplementary Figure 1.



**Extended Data Figure 5. TASL mirrors SLC15A4 requirement for TLR7/8 activation.**  
**(a)** Fraction of R848-induced genes affected by *SLC15A4* and *TASL* knockout, related to Fig. 2b. **(b)** Upset plot representing number of R848-induced genes commonly affected by indicated sgRNAs, related to Fig. 2b. **(c)** *TASL* gene expression levels in indicated THP1 cells, related to Fig. 2b. Bar graphs shown mean (n=3 biological replicates), error bars show 95 % confidence interval of mean. **(d)** Flow cytometry of PD-L1 surface expression in indicated unstimulated (ns) or R848-stimulated (5 μg/ml, 24h) THP1 cells. **(e)** Immunoblots of indicated THP1 DUAL cells. Lysates treated with PNGase F as indicated. **(f-i,k)** Indicated

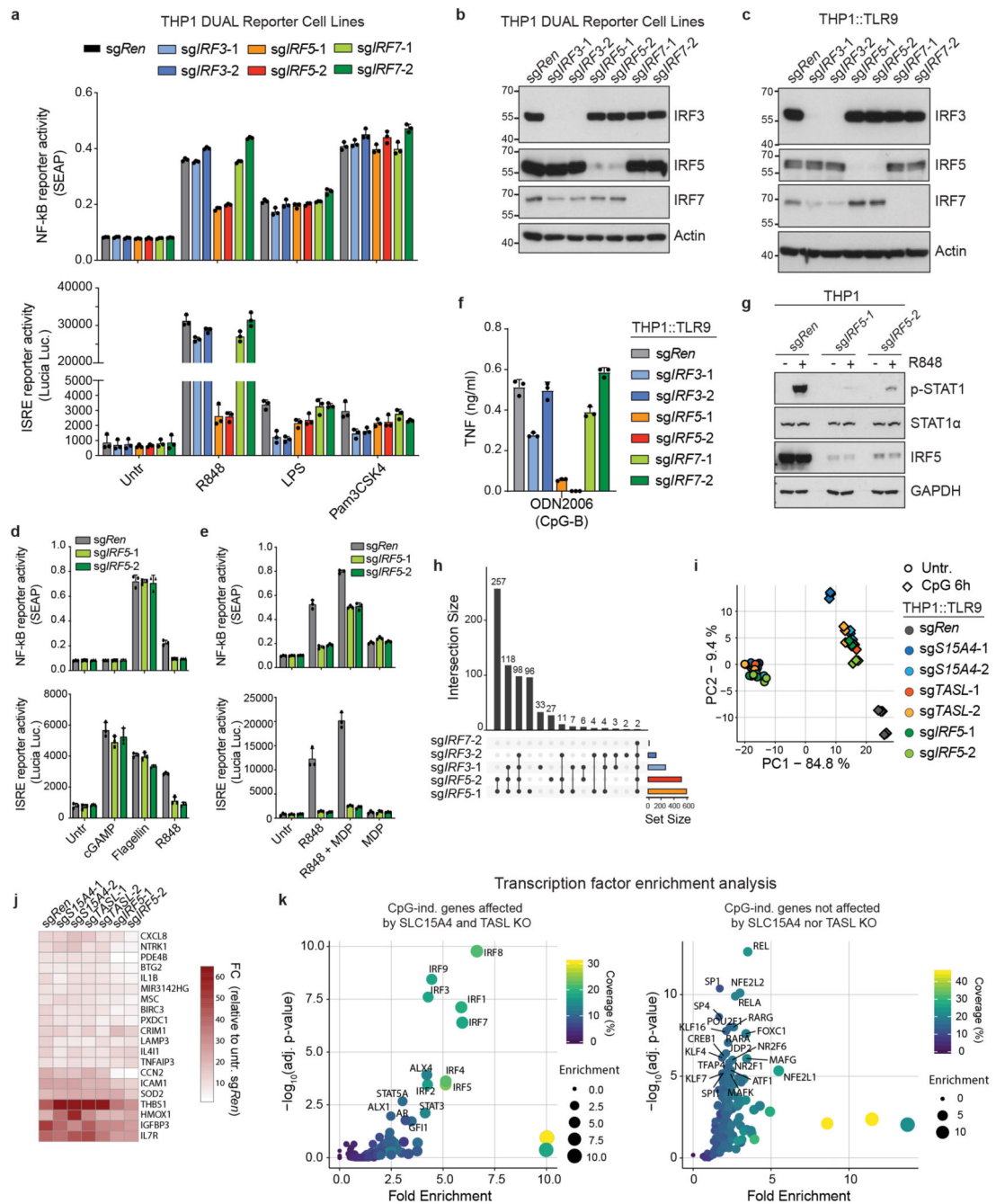
THP1 DUAL cells were (co-)treated for 24 hours with R848 (5 µg/ml), CL075 (5 µg/ml), ssRNA40/LyoVec™ (5 µg/ml) or inactive control ssRNA41/LyoVec™ (5 µg/ml), C12-iE-DAP (5 µg/ml), MDP (10 µg/ml), murabutide (10 µg/ml), Pam3CSK4 (0.1 µg/ml), Flagellin (0.1 µg/ml), cGAMP (3 µg/ml) or interferon β (20 ng/ml). **(h)** CRISPR/Cas9 editing efficiency (%) estimated by TIDE. **(j)** Indicated THP1 DUAL cells were primed or not with interferon γ (0.1 µg/ml) for 24h, washed and stimulated or not with MDP (10 µg/ml, 24h). **(f-k)** Supernatants were analyzed for ISRE and NF-κB reporter activity. Mean ± s.d. (n=3 biological replicates). **(l)** Relative mRNA expression of *SLC15A4*, *TASL* or *MYD88* in siRNA-transfected CD14<sup>+</sup> monocytes in comparison to control (siCTRL). Data represent mean ± s.d. from six (*MYD88*, n=6) or seven (*SLC15A4*, *TASL*, n=7) individual donors. **(d-k)** Data representative of two independent experiments. For gel source data, see Supplementary Figure 1.



**Extended Data Figure 6. TASL and SLC15A4 deficiency impairs endosomal TLR-mediated signaling downstream of receptor engagement.**

**(a)** Immunoblots of lysates of THP1 cells treated with PNGase F as indicated. **(b,c)** Cytokine production of indicated THP1 cells unstimulated or stimulated with CpG-A, CpG-B (5  $\mu$ M) or R848 (5  $\mu$ g/ml) for 24h. Data show mean  $\pm$  s.d. of biological replicates (TNF, CCL2: n=3; IFN  $\beta$ : n=2). **(d)** Immunoblots of indicated THP1 cells stimulated or not with interferon  $\gamma$  (0.1  $\mu$ g/ml, 16h). **(e)** Immunoblots of indicated THP1 cells. **(f)** Indicated THP1::TLR9 cells treated with FITC-labeled CpG-A or CpG-B (1  $\mu$ M, 0-120 min.) were

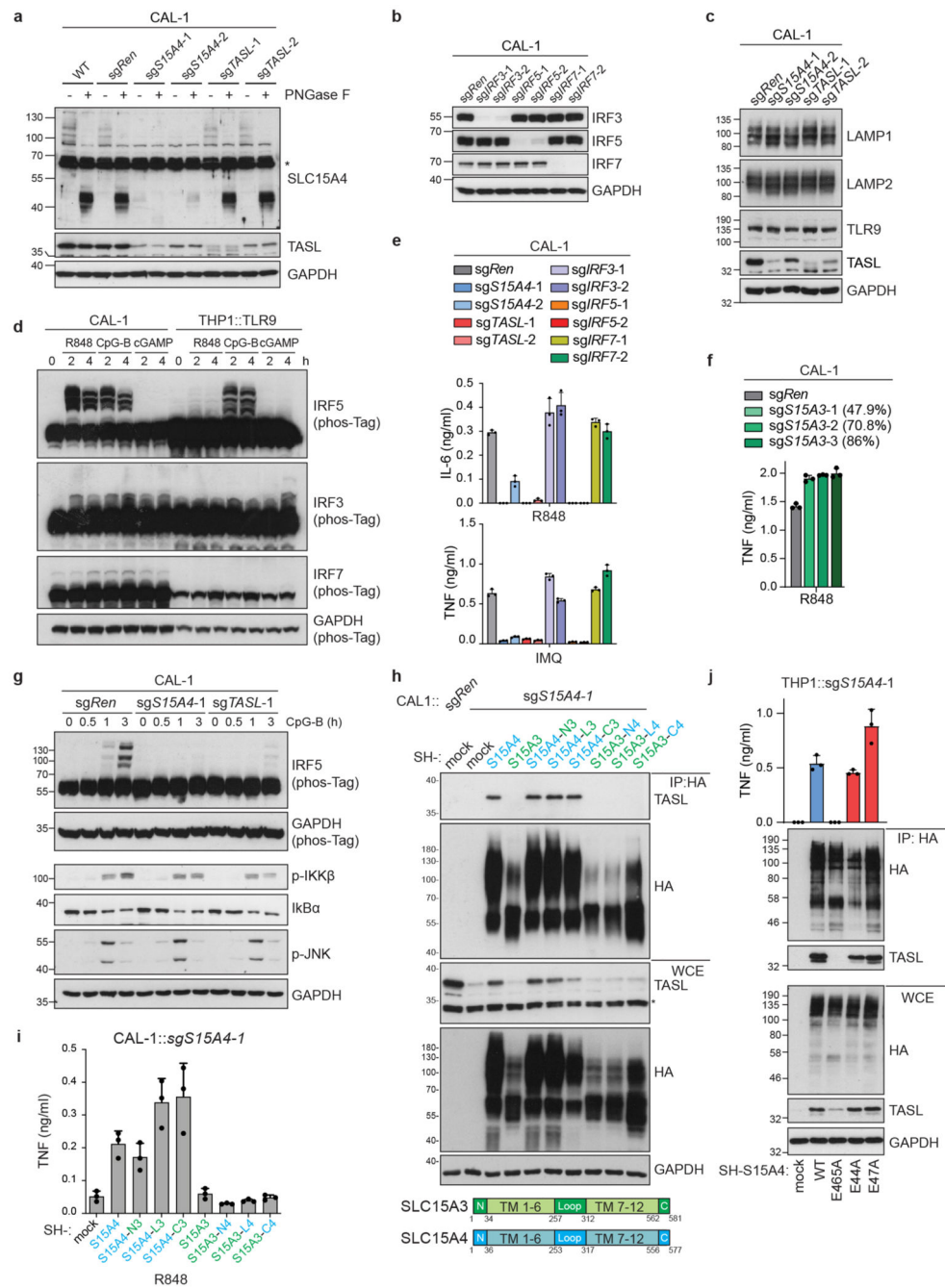
analyzed by flow cytometry. **(g)** Representative flow cytometry scatter plots of phagocytosis assays. Differentiated THP1 cells, treated or not with Bafilomycin A1, were incubated with dual-colored opsonized beads. Using intensities of pH-insensitive (YG) and pH-sensitive (pHrodo-Red, signal increases with decrease in pH) dyes, cells are divided into phagocytosis negative (PhagoNeg: double-negative), cells that have undergone phagocytosis and phagosome acidification (PhagoLate: double-positive) and early phagocytic cells (PhagoEarly: YG and low pHrodo-Red signal). The marginal intensity distributions are displayed on the sides of the plot. **(h)** Bar graphs show mean  $\pm$  s.d. (n=3 biological replicates) of fractions described in **(g)**. **(i,j)** Indicated THP1 cells were subjected to phagocytosis assays. **(i)** Bar graphs show mean  $\pm$  s.d. (n=3 biological replicates) of fractions described in **(g)**. **(j)** Bar graphs represent mean MFI  $\pm$  s.d. (n=3 biological replicates) of the pHrodo-Red signal acquired in the MFI gate shown in **(g)** focusing on cells having taken up 1 to 3 beads/cell. **(k)** Flow diagram for quantification of Lysosensor™ Green intensities in lysosomal compartments by microscopy. Box plots show intensity of Lysosensor signal on LysoTracker positive lysosomes, as measured by imaging in the indicated THP1 cells. Bars indicate median, boxes the first–third quartiles. Upper whisker extends from hinge to largest value no further than 1.5 \* IQR (inter-quartile range) from the hinge. Lower from hinge to smallest value at most 1.5 \* IQR of the hinge. Outliers are shown as circles. *sgRerr*: n=2432, *sgSLC15A4-1*: n=1721, *sgSLC15A4-2*: n=1981, *sgTASL-1*: n=2378, *sgTASL-2*: n=2627 quantified speckles. **(l)** Immunoblots of indicated THP1 cells stimulated with R848 (5  $\mu$ g/ml, 0-180 min.). **(a-k)** Data representative of **(a-f,k,l)** two or **(g-j)** three independent experiments. For gel source data, see Supplementary Figure 1.



**Extended Data Figure 7. TASL/SLC15A4 loss mirrors IRF5-deficiency in perturbing endosomal TLR responses.**

(a,d,e) THP1 DUAL cells were (co-)treated for 24 hours with R848 (5 µg/ml), LPS (0.1 µg/ml), Pam3CSK4 (0.1 µg/ml), cGAMP (3 µg/ml), Flagellin (0.1 µg/ml) or MDP (10 µg/ml) as indicated. Supernatants were analyzed for ISRE and NF-κB reporter activity. (b,c) Immunoblots of indicated (b) THP1 DUAL or (c) THP1::TLR9 cells. (f) TNF production of indicated THP1::TLR9 cells stimulated with CpG-B (2 µM, 24h). (g) Immunoblots of indicated THP1 cells stimulated or not with R848 (5 µg/ml, 3h). (h) Upset plot representing

number of CpG-B-induced genes (2  $\mu$ M, 6h; DESeq2 adjusted p-value < 0.05, n=3 biological replicates) in comparison to control (sg*Ren*) commonly affected by indicated sgRNAs. No gene was significantly affected by sg*IRF7-1*. **(i)** PCA plot of transcriptional profiles of untreated and CpG-B-treated (2  $\mu$ M, 6h) THP1::TLR9 cells (n=3 biological replicates) shown in Fig. 3d. **(j)** Heatmap representing 20 most induced genes by CpG-B in control THP1::TLR9 cells and not affected by neither *SLC15A4*, *TASL* nor *IRF5* knockout, related to Fig. 3d,e. **(k)** Transcription factor enrichment analysis (two-sided Fisher's Exact Test, p-value adjusted for multiple testing) of genes upregulated upon CpG-B treatment in control THP1 cells specifically affected (DESeq2 adjusted p-value < 0.05, n=3 biological replicates) (left panel) or not (right panel) by *SLC15A4* and *TASL* knockout, related to Fig. 3d,e. Background sets are defined as all genes upregulated by CpG-B treatment or all expressed genes (counts per million > 1) respectively. **(a,d-f)** Data show mean  $\pm$  s.d. (n=3 biological replicates). **(a-g)** Data representative of two independent experiments. For gel source data, see Supplementary Figure 1.

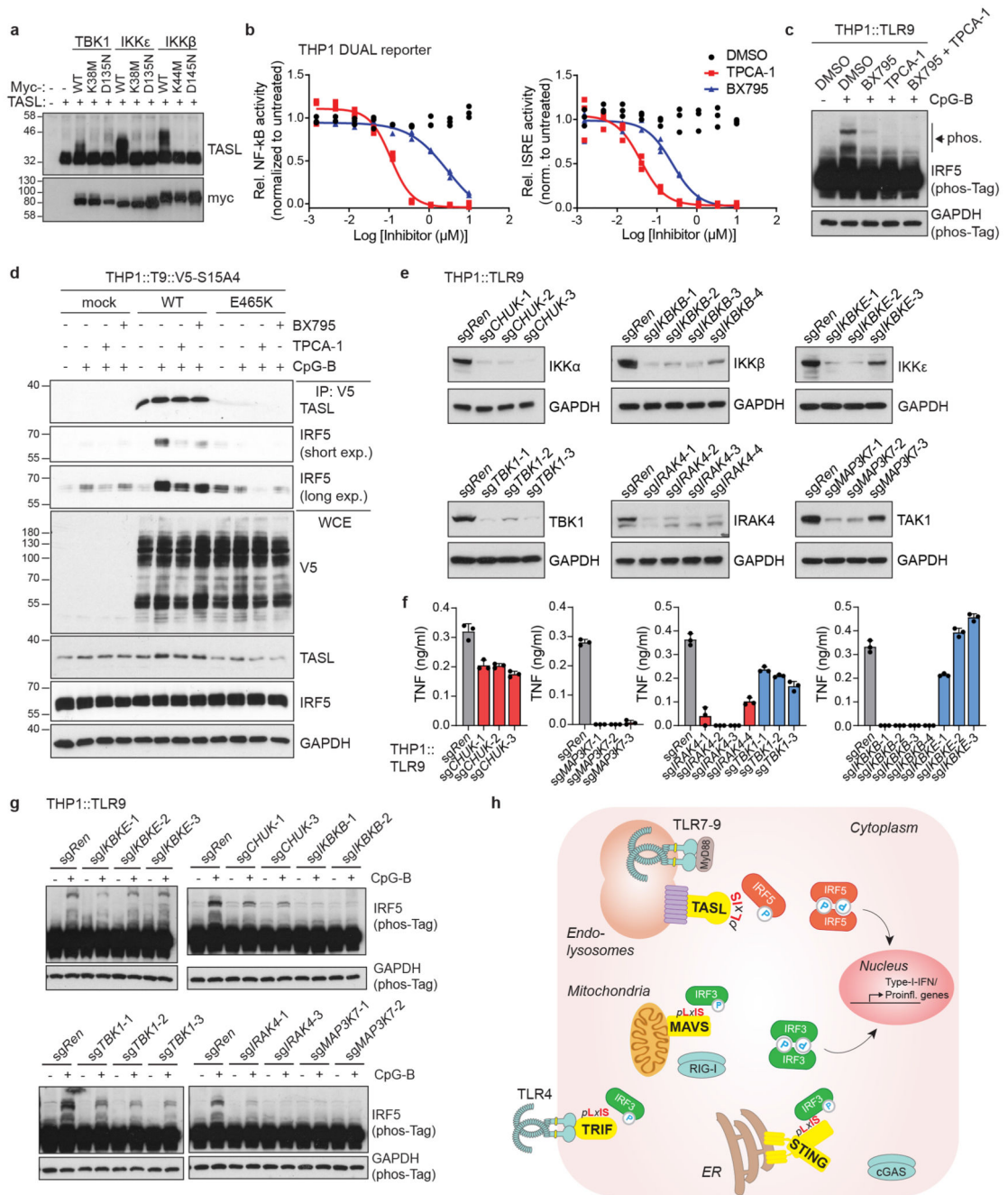


**Extended Data Figure 8. SLC15A4/TASL complex is required for IRF5-dependent signaling in human pDC CAL-1 cells.**

(a-c) Immunoblots of lysates of CAL-1 cells, PNGase F treatment as indicated. (d) Immunoblots of CAL-1 or THP1::TLR9 cells stimulated with R848 (5 μg/ml), CpG-B (5 μM) or cGAMP (3 μg/ml) as indicated. (e,f) Cytokine production of indicated CAL-1 cells stimulated with R848 (5 μg/ml) or imiquimod (IMQ, 5 μg/ml) for 24h. (f) CRISPR/Cas9 editing efficiency (%) estimated by TIDE. (g) Immunoblots of CAL-1 cells stimulated with CpG-B (5 μM, 0-180 min.) as indicated. (h) Lysates from indicated CAL-1 cells were



(a) Overview of mutants used in Fig. 4b, changes to alanine indicated by red circles. (b,f) Immunoblots of indicated THP1 cells. Bar graphs represent TNF levels following R848 stimulation (5  $\mu$ g/ml, 24h). (f) Dashed line indicates cropping of unrelated lanes from the same blots. (c) Immunoblots of indicated reconstituted *TASL*-deficient THP1 cells. (d) Normal expression levels, but reduced detection by anti-TASL antibodies of TASL mutants targeting aa 261-277. Immunoblots of HEK293T cells transiently transfected with indicated cDNAs. (e) Lysates from indicated THP1 cells were subjected to immunoprecipitation (IP). IP and whole cell extracts (WCE) were analyzed by immunoblotting. (g) Abundance of indicated proteins determined by MS in V5-immunoprecipitates from THP1::TLR9 cells stimulated with CpG-B (5  $\mu$ M, 2h) as indicated, related to Fig. 4g. Three biological replicates are shown. (h) Crystal structures of IRF3 bound to phosphorylated *pLxIS*-containing peptides from STING (pink, PDB ID 5JEJ), MAVS (green, PDB ID 5JEK) and TRIF (blue, PDB ID 5JEL). Residues in STING peptides shown as sticks. (i) Superposition of peptide-bound IRF3 (PDB ID 5JEJ) and dimeric IRF5 (one monomer shown, PDB ID 3DSH), showing highly similar folds. (j) Model of phosphomimetic *pLxIS*-containing peptide from TASL (pmTASL, ISTPSLHIDQYSNV, yellow) bound to IRF5. Residues corresponding to LxIS motif shown as sticks. (k) Comparison of binding mode of *pLxIS*-containing peptides to IRF proteins. Only IRF5 is shown for clarity. (l) Immunoblots of indicated THP1 cells unstimulated or stimulated with R848 (5  $\mu$ g/ml, 2h). (m) TNF production of cells described in (l) stimulated with R848 (5  $\mu$ g/ml, 24h). (b,f,m) Bar graphs show mean  $\pm$  s.d. (n=3 biological replicates). (b-f,l,m) Data are representative of two independent experiments. For gel source data, see Supplementary Figure 1.



**Extended Data Figure 10. IKKβ is required for TASL-dependent IRF5 activation.**

(a) Immunoblots of HEK293T cells transfected as indicated. (b) THP1 DUAL cells were pre-treated for 30 min. with DMSO or inhibitors as indicated and stimulated with R848 (5 μg/ml, 24h). Supernatants were analyzed for ISRE and NF-κB reporter activity and normalized to the respective R848-only treated conditions. Three biological replicates are shown (n=3). (c) Immunoblots of THP1::TLR9 cells pre-treated for 30 min. with DMSO or inhibitors (5 μM) and stimulated with CpG-B (5 μM, 4h) as indicated. (d) Lysates from THP1::TLR9 cells pre-treated (30 min.) with DMSO or inhibitors (5 μM) and stimulated

with CpG-B (5  $\mu$ M, 2h) as indicated were subjected to V5-immunoprecipitation. Immunoprecipitates (IP) and whole cell extracts (WCE) were analyzed by immunoblotting. (e) Immunoblots of indicated THP1::TLR9 cells. *CHUK* gene encodes for IKK $\alpha$ , *MAP3K7* for TAK1 protein. (f) TNF production of indicated THP1::TLR9 cells stimulated with CpG-B (2  $\mu$ M, 24h). Data show mean  $\pm$  s.d. (n=3 biological replicates). (g) Immunoblots of indicated THP1::TLR9 cells stimulated with CpG-B (5  $\mu$ M, 3h). (h) Schematic model representing functional homology of the SLC15A4-TASL module in mediating IRF5 activation in comparison to IRF3 adaptors STING/MAVS/TRIF. (a-g) Data are representative of two independent experiments. For gel source data, see Supplementary Figure 1.

## Supplementary Material

Refer to Web version on PubMed Central for supplementary material.

## Acknowledgments

We thank all members of the Superti-Furga laboratory, Guido Boehmelt (Boehringer Ingelheim, Vienna, Austria), Thomas Krausgruber (CeMM) and Elisabeth Salzer (LBI-RUD, Vienna Austria) for discussions and feedback, the Proteomics and Metabolomics Facility (CeMM) for the proteomics analyses, the Biomedical Sequencing Facility (CeMM/Medical University of Vienna) for the NGS sequencing and the Core Facility Imaging of the Medical University of Vienna. We thank Prof. Takahiro Maeda (Nagasaki University) for kindly providing the CAL-1 cells. This work was supported by Boehringer Ingelheim (Research Collaboration Agreement BI-CeMM 238114 L.X.H., U.K., K.P, A.S. and M.R.), the Austrian Academy of Sciences (G.S.-F., F.K., V.S., A.C-R), the European Research Council (ERC AdG 695214 GameofGates G.S.-F., M.R., S.S., P.E., U.G., M.D.P., A.B., E.G.) and Austrian Science Fund (FWF SFB F4711, J.W.B.). Plasmids obtained through Addgene were a gift from Feng Zhang, Didier Trono and Doug Golenbock.

## Data availability

TAP-MS proteomics data have been deposited to the ProteomeXchange Consortium<sup>77</sup> via the PRIDE<sup>78</sup> partner repository with the dataset identifier PXD014254 and 10.6019/PXD014254. RNA-Seq data have been deposited to the GEO repository (GSE133317). Source data for immunoblots are provided in Supplementary Figure 1.

## References

- Blasius AL, Beutler B. Intracellular toll-like receptors. *Immunity*. 2010; 32:305–315. DOI: 10.1016/j.immuni.2010.03.012 [PubMed: 20346772]
- Pelka K, Shibata T, Miyake K, Latz E. Nucleic acid-sensing TLRs and autoimmunity: novel insights from structural and cell biology. *Immunol Rev*. 2016; 269:60–75. DOI: 10.1111/imr.12375 [PubMed: 26683145]
- Kawai T, Akira S. The role of pattern-recognition receptors in innate immunity: update on Toll-like receptors. *Nat Immunol*. 2010; 11:373–384. DOI: 10.1038/ni.1863 [PubMed: 20404851]
- Bentham J, et al. Genetic association analyses implicate aberrant regulation of innate and adaptive immunity genes in the pathogenesis of systemic lupus erythematosus. *Nat Genet*. 2015; 47:1457–1464. DOI: 10.1038/ng.3434 [PubMed: 26502338]
- Odhams CA, et al. Interferon inducible X-linked gene CXorf21 may contribute to sexual dimorphism in Systemic Lupus Erythematosus. *Nat Commun*. 2019; 10:2164 doi: 10.1038/s41467-019-10106-2 [PubMed: 31092820]

6. Han JW, et al. Genome-wide association study in a Chinese Han population identifies nine new susceptibility loci for systemic lupus erythematosus. *Nat Genet.* 2009; 41:1234–1237. DOI: 10.1038/ng.472 [PubMed: 19838193]
7. Blasius AL, et al. Slc15a4, AP-3, and Hermansky-Pudlak syndrome proteins are required for Toll-like receptor signaling in plasmacytoid dendritic cells. *Proc Natl Acad Sci U S A.* 2010; 107:19973–19978. DOI: 10.1073/pnas.1014051107 [PubMed: 21045126]
8. Sasawatari S, et al. The solute carrier family 15A4 regulates TLR9 and NOD1 functions in the innate immune system and promotes colitis in mice. *Gastroenterology.* 2011; 140:1513–1525. DOI: 10.1053/j.gastro.2011.01.041 [PubMed: 21277849]
9. Kobayashi T, et al. The histidine transporter SLC15A4 coordinates mTOR-dependent inflammatory responses and pathogenic antibody production. *Immunity.* 2014; 41:375–388. DOI: 10.1016/j.immuni.2014.08.011 [PubMed: 25238095]
10. Liu S, et al. Phosphorylation of innate immune adaptor proteins MAVS, STING, and TRIF induces IRF3 activation. *Science.* 2015; 347:aaa2630 doi: 10.1126/science.aaa2630 [PubMed: 25636800]
11. Zhao B, et al. Structural basis for concerted recruitment and activation of IRF-3 by innate immune adaptor proteins. *Proc Natl Acad Sci U S A.* 2016; 113:E3403–3412. DOI: 10.1073/pnas.1603269113 [PubMed: 27302953]
12. Tsokos GC. Systemic lupus erythematosus. *N Engl J Med.* 2011; 365:2110–2121. DOI: 10.1056/NEJMra1100359 [PubMed: 22129255]
13. Moulton VR, et al. Pathogenesis of Human Systemic Lupus Erythematosus: A Cellular Perspective. *Trends Mol Med.* 2017; 23:615–635. DOI: 10.1016/j.molmed.2017.05.006 [PubMed: 28623084]
14. Tsokos GC, Lo MS, Costa Reis P, Sullivan KE. New insights into the immunopathogenesis of systemic lupus erythematosus. *Nat Rev Rheumatol.* 2016; 12:716–730. DOI: 10.1038/nrrheum.2016.186 [PubMed: 27872476]
15. Kieser KJ, Kagan JC. Multi-receptor detection of individual bacterial products by the innate immune system. *Nat Rev Immunol.* 2017; 17:376–390. DOI: 10.1038/nri.2017.25 [PubMed: 28461704]
16. Janeway CA Jr, Medzhitov R. Innate immune recognition. *Annu Rev Immunol.* 2002; 20:197–216. DOI: 10.1146/annurev.immunol.20.083001.084359 [PubMed: 11861602]
17. O’Neill LA, Golenbock D, Bowie AG. The history of Toll-like receptors - redefining innate immunity. *Nat Rev Immunol.* 2013; 13:453–460. DOI: 10.1038/nri3446 [PubMed: 23681101]
18. Blasius AL, Krebs P, Sullivan BM, Oldstone MB, Popkin DL. Slc15a4, a gene required for pDC sensing of TLR ligands, is required to control persistent viral infection. *PLoS Pathog.* 2012; 8:e1002915 doi: 10.1371/journal.ppat.1002915 [PubMed: 23028315]
19. Baccala R, et al. Essential requirement for IRF8 and SLC15A4 implicates plasmacytoid dendritic cells in the pathogenesis of lupus. *Proc Natl Acad Sci U S A.* 2013; 110:2940–2945. DOI: 10.1073/pnas.1222798110 [PubMed: 23382217]
20. Dosenovic P, et al. Slc15a4 function is required for intact class switch recombination to IgG2c in response to TLR9 stimulation. *Immunol Cell Biol.* 2015; 93:136–146. DOI: 10.1038/icb.2014.82 [PubMed: 25310967]
21. Griffith AD, et al. A requirement for slc15a4 in imiquimod-induced systemic inflammation and psoriasiform inflammation in mice. *Sci Rep.* 2018; 8:14451 doi: 10.1038/s41598-018-32668-9 [PubMed: 30262916]
22. Langefeld CD. Transancestral mapping and genetic load in systemic lupus erythematosus. *Nat Commun.* 2017; 8:16021 doi: 10.1038/ncomms16021 [PubMed: 28714469]
23. Pollard KM, et al. Induction of Systemic Autoimmunity by a Xenobiotic Requires Endosomal TLR Trafficking and Signaling from the Late Endosome and Endolysosome but Not Type I IFN. *J Immunol.* 2017; 199:3739–3747. DOI: 10.4049/jimmunol.1700332 [PubMed: 29055005]
24. Rebsamen M, et al. SLC38A9 is a component of the lysosomal amino acid sensing machinery that controls mTORC1. *Nature.* 2015; 519:477–481. DOI: 10.1038/nature14107 [PubMed: 25561175]
25. Pichlmair A, et al. Viral immune modulators perturb the human molecular network by common and unique strategies. *Nature.* 2012; 487:486–490. DOI: 10.1038/nature11289 [PubMed: 22810585]

26. Nakamura N, et al. Endosomes are specialized platforms for bacterial sensing and NOD2 signalling. *Nature*. 2014; 509:240–244. DOI: 10.1038/nature13133 [PubMed: 24695226]
27. Harris VM, Harley ITW, Kurien BT, Koelsch KA, Scofield RH. Lysosomal pH Is Regulated in a Sex Dependent Manner in Immune Cells Expressing CXorf21. *Front Immunol*. 2019; 10:578. doi: 10.3389/fimmu.2019.00578 [PubMed: 31001245]
28. Libert C, Dejager L, Pinheiro I. The X chromosome in immune functions: when a chromosome makes the difference. *Nat Rev Immunol*. 2010; 10:594–604. DOI: 10.1038/nri2815 [PubMed: 20651746]
29. Klijn C, et al. A comprehensive transcriptional portrait of human cancer cell lines. *Nat Biotechnol*. 2015; 33:306–312. DOI: 10.1038/nbt.3080 [PubMed: 25485619]
30. FANTOM Consortium and the RIKEN PMI and CLST. A promoter-level mammalian expression atlas. *Nature*. 2014; 507:462–470. [PubMed: 24670764]
31. Arazi A, et al. The immune cell landscape in kidneys of patients with lupus nephritis. *Nat Immunol*. 2019; 20:902–914. DOI: 10.1038/s41590-019-0398-x [PubMed: 31209404]
32. Muskardin TLW, Niewold TB. Type I interferon in rheumatic diseases. *Nat Rev Rheumatol*. 2018; 14:214–228. DOI: 10.1038/nrrheum.2018.31 [PubMed: 29559718]
33. Hu Y, Song F, Jiang H, Nunez G, Smith DE. SLC15A2 and SLC15A4 Mediate the Transport of Bacterially Derived Di/Tripeptides To Enhance the Nucleotide-Binding Oligomerization Domain-Dependent Immune Response in Mouse Bone Marrow-Derived Macrophages. *J Immunol*. 2018; 201:652–662. DOI: 10.4049/jimmunol.1800210 [PubMed: 29784761]
34. Lee J, et al. pH-dependent internalization of muramyl peptides from early endosomes enables Nod1 and Nod2 signaling. *J Biol Chem*. 2009; 284:23818–23829. DOI: 10.1074/jbc.M109.033670 [PubMed: 19570976]
35. Chow KT, et al. Differential and Overlapping Immune Programs Regulated by IRF3 and IRF5 in Plasmacytoid Dendritic Cells. *J Immunol*. 2018; 201:3036–3050. DOI: 10.4049/jimmunol.1800221 [PubMed: 30297339]
36. Graham RR, et al. A common haplotype of interferon regulatory factor 5 (IRF5) regulates splicing and expression and is associated with increased risk of systemic lupus erythematosus. *Nat Genet*. 2006; 38:550–555. DOI: 10.1038/ng1782 [PubMed: 16642019]
37. Schoenemeyer A, et al. The interferon regulatory factor, IRF5, is a central mediator of toll-like receptor 7 signaling. *J Biol Chem*. 2005; 280:17005–17012. DOI: 10.1074/jbc.M412584200 [PubMed: 15695821]
38. Takaoka A, et al. Integral role of IRF-5 in the gene induction programme activated by Toll-like receptors. *Nature*. 2005; 434:243–249. DOI: 10.1038/nature03308 [PubMed: 15665823]
39. Eames HL, Corbin AL, Udalova IA. Interferon regulatory factor 5 in human autoimmunity and murine models of autoimmune disease. *Transl Res*. 2016; 167:167–182. DOI: 10.1016/j.trsl.2015.06.018 [PubMed: 26207886]
40. Maeda T, et al. A novel plasmacytoid dendritic cell line, CAL-1, established from a patient with blastic natural killer cell lymphoma. *Int J Hematol*. 2005; 81:148–154. DOI: 10.1532/ijh97.04116 [PubMed: 15765784]
41. Steinhagen F, et al. IRF-5 and NF-kappaB p50 co-regulate IFN-beta and IL-6 expression in TLR9-stimulated human plasmacytoid dendritic cells. *Eur J Immunol*. 2013; 43:1896–1906. DOI: 10.1002/eji.201242792 [PubMed: 23616277]
42. Newstead S. Recent advances in understanding proton coupled peptide transport via the POT family. *Curr Opin Struct Biol*. 2017; 45:17–24. DOI: 10.1016/j.sbi.2016.10.018 [PubMed: 27865112]
43. Kelley LA, Mezulis S, Yates CM, Wass MN, Sternberg MJ. The Phyre2 web portal for protein modeling, prediction and analysis. *Nat Protoc*. 2015; 10:845–858. DOI: 10.1038/nprot.2015.053 [PubMed: 25950237]
44. Chen W, et al. Insights into interferon regulatory factor activation from the crystal structure of dimeric IRF5. *Nat Struct Mol Biol*. 2008; 15:1213–1220. DOI: 10.1038/nsmb.1496 [PubMed: 18836453]

45. Lopez-Pelaez M, et al. Protein kinase IKKbeta-catalyzed phosphorylation of IRF5 at Ser462 induces its dimerization and nuclear translocation in myeloid cells. *Proc Natl Acad Sci U S A*. 2014; 111:17432–17437. DOI: 10.1073/pnas.1418399111 [PubMed: 25326418]
46. Ren J, Chen X, Chen ZJ. IKKbeta is an IRF5 kinase that instigates inflammation. *Proc Natl Acad Sci U S A*. 2014; 111:17438–17443. DOI: 10.1073/pnas.1418516111 [PubMed: 25326420]
47. Doench JG, et al. Optimized sgRNA design to maximize activity and minimize off-target effects of CRISPR-Cas9. *Nat Biotechnol*. 2016; 34:184–191. DOI: 10.1038/nbt.3437 [PubMed: 26780180]
48. Bigenzahn JW, et al. LZTR1 is a regulator of RAS ubiquitination and signaling. *Science*. 2018; 362:1171–1177. DOI: 10.1126/science.aap8210 [PubMed: 30442766]
49. Brinkman EK, Chen T, Amendola M, van Steensel B. Easy quantitative assessment of genome editing by sequence trace decomposition. *Nucleic Acids Res*. 2014; 42 e168 doi: 10.1093/nar/gku936 [PubMed: 25300484]
50. Troegeler A, et al. An efficient siRNA-mediated gene silencing in primary human monocytes, dendritic cells and macrophages. *Immunol Cell Biol*. 2014; 92:699–708. DOI: 10.1038/icb.2014.39 [PubMed: 24890643]
51. Rudashevskaya EL, et al. A method to resolve the composition of heterogeneous affinity-purified protein complexes assembled around a common protein by chemical cross-linking, gel electrophoresis and mass spectrometry. *Nat Protoc*. 2013; 8:75–97. DOI: 10.1038/nprot.2012.133 [PubMed: 23237831]
52. Varjosalo M, et al. Interlaboratory reproducibility of large-scale human protein-complex analysis by standardized AP-MS. *Nat Methods*. 2013; 10:307–314. DOI: 10.1038/nmeth.2400 [PubMed: 23455922]
53. Olsen JV, et al. Parts per million mass accuracy on an Orbitrap mass spectrometer via lock mass injection into a C-trap. *Mol Cell Proteomics*. 2005; 4:2010–2021. DOI: 10.1074/mcp.T500030-MCP200 [PubMed: 16249172]
54. Chambers MC, et al. A cross-platform toolkit for mass spectrometry and proteomics. *Nat Biotechnol*. 2012; 30:918–920. DOI: 10.1038/nbt.2377 [PubMed: 23051804]
55. Apweiler R, et al. UniProt: the Universal Protein knowledgebase. *Nucleic Acids Res*. 2004; 32:D115–119. DOI: 10.1093/nar/gkh131 [PubMed: 14681372]
56. Cox J, Mann M. MaxQuant enables high peptide identification rates, individualized p.p.b.-range mass accuracies and proteome-wide protein quantification. *Nat Biotechnol*. 2008; 26:1367–1372. DOI: 10.1038/nbt.1511 [PubMed: 19029910]
57. Wright JC, Choudhary JS. DecoyPyrat: Fast Non-redundant Hybrid Decoy Sequence Generation for Large Scale Proteomics. *J Proteomics Bioinform*. 2016; 9:176–180. DOI: 10.4172/jpb.1000404 [PubMed: 27418748]
58. Kim S, Pevzner PA. MS-GF+ makes progress towards a universal database search tool for proteomics. *Nat Commun*. 2014; 5 5277 doi: 10.1038/ncomms6277 [PubMed: 25358478]
59. Elias JE, Gygi SP. Target-decoy search strategy for increased confidence in large-scale protein identifications by mass spectrometry. *Nat Methods*. 2007; 4:207–214. DOI: 10.1038/nmeth1019 [PubMed: 17327847]
60. The M, MacCoss MJ, Noble WS, Kall L. Fast and Accurate Protein False Discovery Rates on Large-Scale Proteomics Data Sets with Percolator 3.0. *J Am Soc Mass Spectrom*. 2016; 27:1719–1727. DOI: 10.1007/s13361-016-1460-7 [PubMed: 27572102]
61. Choi H, et al. Analyzing protein-protein interactions from affinity purification-mass spectrometry data with SAINT. *Curr Protoc Bioinformatics*. 2012; doi: 10.1002/0471250953.bi0815s39
62. Shannon P, et al. Cytoscape: a software environment for integrated models of biomolecular interaction networks. *Genome Res*. 2003; 13:2498–2504. DOI: 10.1101/gr.1239303 [PubMed: 14597658]
63. Mellacheruvu D, et al. The CRAPome: a contaminant repository for affinity purification-mass spectrometry data. *Nat Methods*. 2013; 10:730–736. DOI: 10.1038/nmeth.2557 [PubMed: 23921808]
64. UniProt C. UniProt: a worldwide hub of protein knowledge. *Nucleic Acids Res*. 2019; 47:D506–D515. DOI: 10.1093/nar/gky1049 [PubMed: 30395287]

65. Larkin MA, et al. Clustal W and Clustal X version 2.0. *Bioinformatics*. 2007; 23:2947–2948. DOI: 10.1093/bioinformatics/btm404 [PubMed: 17846036]
66. Drozdetskiy A, Cole C, Procter J, Barton GJ. JPred4: a protein secondary structure prediction server. *Nucleic Acids Res*. 2015; 43:W389–394. DOI: 10.1093/nar/gkv332 [PubMed: 25883141]
67. Dobin A, et al. STAR: ultrafast universal RNA-seq aligner. *Bioinformatics*. 2013; 29:15–21. DOI: 10.1093/bioinformatics/bts635 [PubMed: 23104886]
68. Derr A, et al. End Sequence Analysis Toolkit (ESAT) expands the extractable information from single-cell RNA-seq data. *Genome Res*. 2016; 26:1397–1410. DOI: 10.1101/gr.207902.116 [PubMed: 27470110]
69. Love MI, Huber W, Anders S. Moderated estimation of fold change and dispersion for RNA-seq data with DESeq2. *Genome Biol*. 2014; 15:550. doi: 10.1186/s13059-014-0550-8 [PubMed: 25516281]
70. Marbach D, et al. Tissue-specific regulatory circuits reveal variable modular perturbations across complex diseases. *Nat Methods*. 2016; 13:366–370. DOI: 10.1038/nmeth.3799 [PubMed: 26950747]
71. Hochberg Y, Benjamini Y. Controlling the false discovery rate: A Practical and powerful approach to multiple testing. *J Roy Statist Soc*. 1995; 57:289–300.
72. Huang da W, Sherman BT, Lempicki RA. Systematic and integrative analysis of large gene lists using DAVID bioinformatics resources. *Nat Protoc*. 2009; 4:44–57. DOI: 10.1038/nprot.2008.211 [PubMed: 19131956]
73. Blaszczyk M, Ciemny MP, Kolinski A, Kurcinski M, Kmiecik S. Protein-peptide docking using CABS-dock and contact information. *Brief Bioinform*. 2018; doi: 10.1093/bib/bby080
74. London N, Raveh B, Cohen E, Fathi G, Schueler-Furman O. Rosetta FlexPepDock web server--high resolution modeling of peptide-protein interactions. *Nucleic Acids Res*. 2011; 39:W249–253. DOI: 10.1093/nar/gkr431 [PubMed: 21622962]
75. Colas C, et al. An improved flow cytometry assay to monitor phagosome acidification. *J Immunol Methods*. 2014; 412:1–13. DOI: 10.1016/j.jim.2014.06.008 [PubMed: 24952246]
76. Carpenter AE, et al. CellProfiler: image analysis software for identifying and quantifying cell phenotypes. *Genome Biol*. 2006; 7 R100 doi: 10.1186/gb-2006-7-10-r100 [PubMed: 17076895]
77. Deutsch EW, et al. The ProteomeXchange consortium in 2017: supporting the cultural change in proteomics public data deposition. *Nucleic Acids Res*. 2017; 45:D1100–D1106. DOI: 10.1093/nar/gkw936 [PubMed: 27924013]
78. Perez-Riverol Y, et al. The PRIDE database and related tools and resources in 2019: improving support for quantification data. *Nucleic Acids Res*. 2019; 47:D442–D450. DOI: 10.1093/nar/gky1106 [PubMed: 30395289]

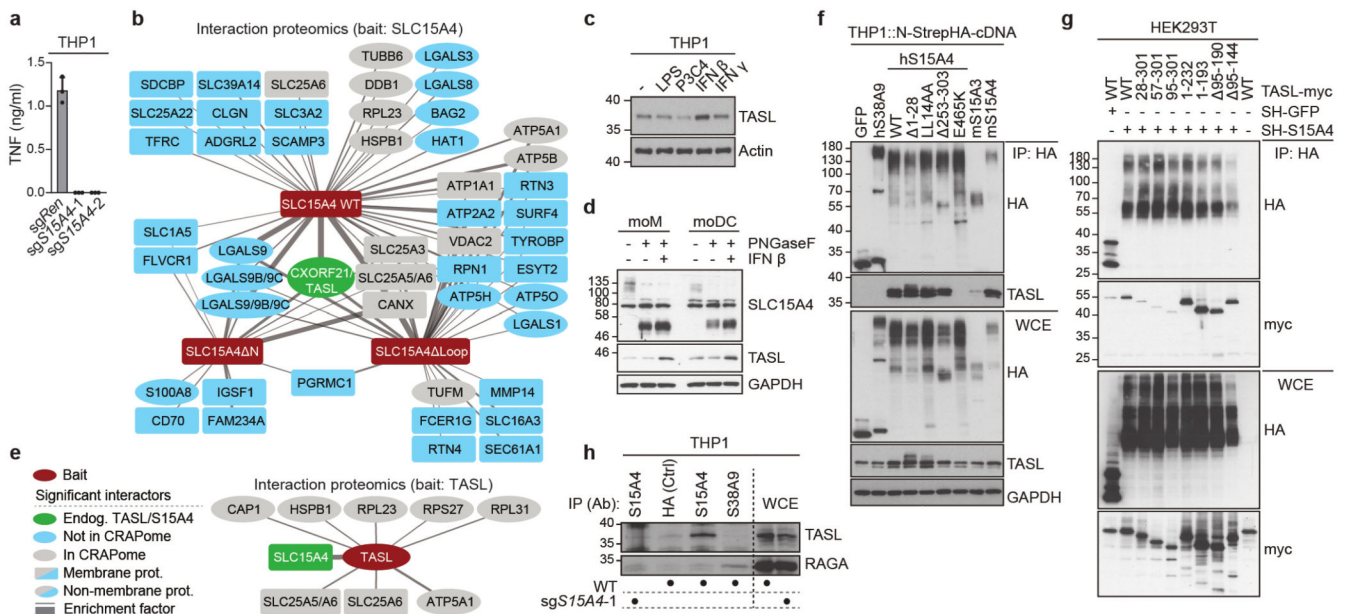


**Figure 1. The type I interferon-inducible protein TASL is a specific interaction partner of SLC15A4.**

(a) TNF production of indicated THP1 cells stimulated with R848 (5 μg/ml, 24h). Mean ± s.d. (n=3 biological replicates). (b,e) Interaction networks of (b) SLC15A4 and deletion mutants and (e) TASL identified by TAP–LC–MS/MS. Baits: red, prey proteins (SAINT FDR <1%): blue or grey if present in CRAPome database. Interactions represented as edges, line width corresponding to enrichment factor calculated by SAINT. (c) Immunoblots of THP1 cells stimulated (16h) with LPS (100 ng/ml), Pam3CSK4 (100 ng/ml), interferon β (20 ng/ml) or interferon γ (20 ng/ml). (d) Immunoblots of lysates from monocyte-derived macrophages (moM) and dendritic cells (moDC) stimulated with interferon β (20 ng/ml, 16h) treated with PNGase F as indicated. (f,g) Immunoprecipitates (IP:HA) and whole cell extracts (WCE) from (f) transduced THP1 or (g) transiently transfected HEK293T cells analyzed by immunoblotting. (h) Immunoprecipitates (IP: indicated antibodies) and WCE from indicated THP1 cells were analyzed by immunoblotting. (a,c-d,f-h) Data representative of (a) five or (c-d,f-h) two independent experiments. For gel source data, see Supplementary Figure 1.

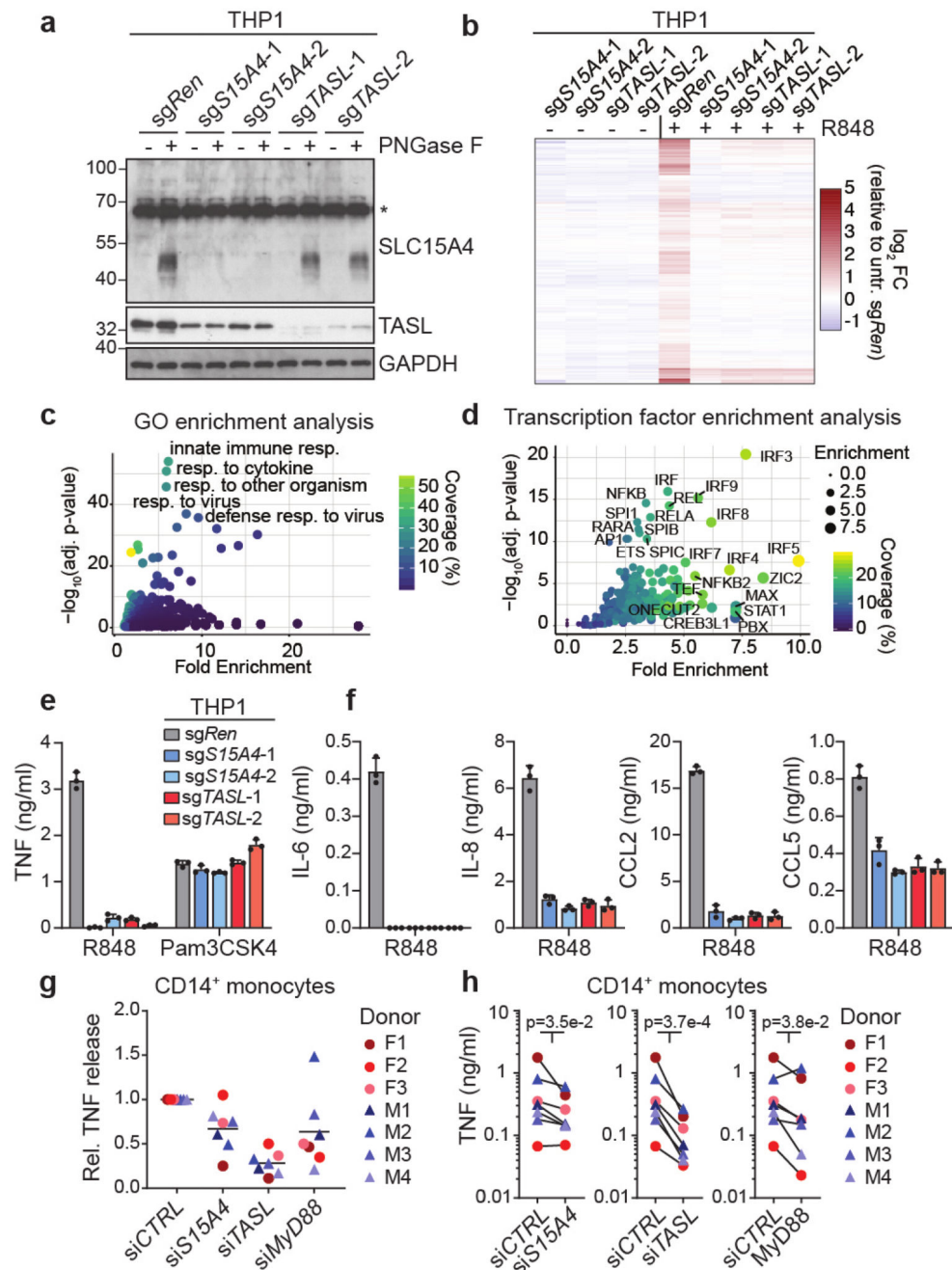


**Figure 2. TASL and SLC15A4 are required for endolysosomal TLR7/8 function.**

(a) Immunoblots of THP1 cell lines. Lysates treated with PNGase F as indicated. (b) Transcriptional profiles of unstimulated and R848-treated (5  $\mu$ g/ml, 6h) THP1 cell lines. Genes significantly up-regulated (FC: fold-change, DESeq2 adjusted p-value < 0.05, n=3 biological replicates) upon R848 treatment in control (*sgRen*) shown. (c) Gene ontology (GO) enrichment analysis (two-sided Fisher's Exact Test, p-value adjusted for multiple testing) for R848-induced genes in control THP1 cells as defined in (b). X-axis: fold enrichment of GO terms in set of upregulated genes compared to all genes expressed (counts

per million > 1). Y-axis: significance of enrichment ( $-\log_{10}$  of p-value adjusted for multiple testing). Color: fraction of R848-induced genes included in corresponding GO term. **(d)** Transcription factor enrichment analysis (two-sided Fisher's Exact Test, p-value adjusted for multiple testing) of R848-induced genes in control THP1 cells as defined in **(b)**. Background set: all expressed genes (counts per million > 1). **(e,f)** Cytokine production of THP1 cells stimulated (24h) with R848 (5  $\mu\text{g/ml}$ ) or Pam3CSK4 (100  $\text{ng/ml}$ ). Mean  $\pm$  s.d. (n=3 biological replicates). **(g,h)** TNF production of siRNA-transfected CD14<sup>+</sup> monocytes stimulated with R848 (5  $\mu\text{g/ml}$ , 24h) from seven healthy donors. F: female, M: male donors. Circles represent **(g)** relative (normalized to siCTRL) or **(h)** absolute TNF levels from seven healthy donors as mean of triplicates (n=7 donors). **(g)** Lines indicate means over seven donors. **(h)** Log<sub>2</sub>-fold changes, relative to siCTRL, of all 7 donors (n=7 donors) tested using paired, two-sided t-test. **(a,e,f)** Data representative of two independent experiments. For gel source data, see Supplementary Figure 1.

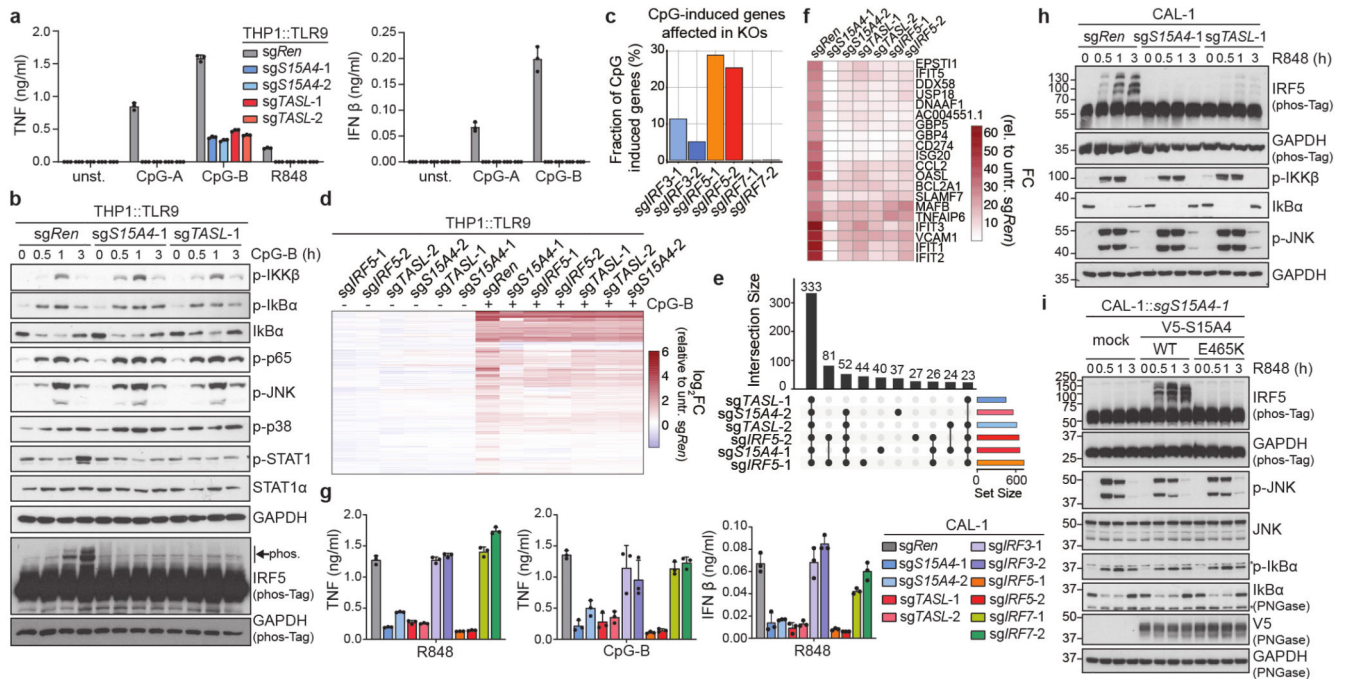


**Figure 3. TASP and SLC15A4 deficiency selectively impairs IRF5-dependent endolysosomal TLR signaling.**

(a) Cytokine production of indicated THP1::TLR9 cells unstimulated or stimulated (24h) with CpG-A/B (5  $\mu$ M) or R848 (5  $\mu$ g/ml). (b) Immunoblots of indicated THP1::TLR9 cells stimulated with CpG-B (5  $\mu$ M, 0-3h). (c) Fraction of CpG-B-induced genes (2  $\mu$ M, 6h; DESeq2 adjusted p-value < 0.05, n=3 biological replicates) affected in *IRF3*, *IRF5* or *IRF7*-deficient THP1::TLR9 cells compared to control (sgRen). (d) Transcriptional profiles of unstimulated and CpG-B-treated (2  $\mu$ M, 6h) THP1::TLR9 cell lines. Genes significantly up-regulated (DESeq2 adjusted p-value < 0.05, n=3 biological replicates) by CpG-B in control (sgRen) shown. (e) Upset plot representing number of CpG-B-induced genes commonly affected by sgRNAs. 10 largest sets shown. (f) Heatmap representing 20 most induced genes by CpG-B in control THP1::TLR9 cells significantly (DESeq2 adjusted p-value < 0.05, n=3 biological replicates) affected by *SLC15A4*, *TASL* and *IRF5* knockout, related to (d,e). (g) Cytokine production of indicated CAL-1 cells stimulated (24h) with R848 (5  $\mu$ g/ml) or CpG-B (5  $\mu$ M). (h,i) Immunoblots of (h) knockout or (i) reconstituted CAL-1 cells stimulated with R848 (5  $\mu$ g/ml, 0-3h) as indicated. (a,g) Mean  $\pm$  s.d. (n=3 biological replicates). (a,b,g,h,i) Data representative of two independent experiments. For gel source data, see Supplementary Figure 1.



sg *TASL-1*. (g) Bait-normalized  $\log_2$ (abundance) of indicated proteins, relative to the mean of unstimulated SLC15A4 E465K samples, determined by MS in V5-immunoprecipitates generated as in (f). Lines indicate median, n=3 biological replicates, two-sided Welch's t-test. (i) R848-induced TNF production (5  $\mu\text{g/ml}$ , 24h), STAT1 and IRF5 phosphorylation (5  $\mu\text{g/ml}$ , 3h) in indicated THP1 cell lines. Lysates were analyzed by immunoblot. (j) Immunoblots of reconstituted CAL-1 cells stimulated with R848 (5  $\mu\text{g/ml}$ , 0-3h). (k) Schematic model of SLC15A4/TASL-dependent IRF5 activation by TLR7-9. (a,i) Bar graphs show mean  $\pm$  s.d. (n=3 biological replicates). (a,f,h-j) Data representative of two independent experiments. For gel source data, see Supplementary Figure 1.